J. theor. Biol. (1987) **124**, 219-250

From Simple to Complex Oscillatory Behaviour: Analysis of Bursting in a Multiply Regulated Biochemical System

OLIVIER DECROLY AND ALBERT GOLDBETER

Faculté des Sciences, Université Libre de Bruxelles, C.P. 231, Campus de la Plaine, B-1050 Brussels, Belgium

(*Received* 1 *May* 1986)

We analyze the transition from simple to complex oscillatory behaviour in a three-variable biochemical system that consists of the coupling in series of two autocatalytic enzyme reactions. Complex periodic behaviour occurs in the form of *bursting* in which clusters of spikes are separated by phases of relative quiescence. The generation of such temporal patterns is investigated by a series of complementary approaches. The dynamics of the system is first cast into two different time-scales, and one of the variables is taken as a slowly-varying parameter influencing the behaviour of the two remaining variables. This analysis shows how complex oscillations develop from simple periodic behaviour and accounts for the existence of various modes of bursting as well as for the dependence of the number of spikes per period on key parameters of the model. We further reduce the number of variables by analyzing bursting by means of one-dimensional return maps obtained from the time evolution of the three-dimensional system. The analysis of a related piecewise linear map allows for a detailed understanding of the complex sequence leading from a bursting pattern with p spikes to a pattern with $p+1$ spikes per period. We show that this transition possesses properties of self-similarity associated with the occurrence of more and more complex patterns of bursting. In addition to bursting, period-doubling bifurcations leading to chaos are observed, as in the differential system, when the piecewise-linear map becomes nonlinear.

1. Introduction

Among the rhythmic patterns of temporal behaviour which are encountered at all levels of biological organization, complex periodic oscillations consisting of *bursts* of several spikes separated by periods of relative quiescence appear to be quite common. Bursting has been observed in nerve cells such as R15 in *Aplysia* (Alving, 1968; Adams & Benson, 1985) or hippocampal neurons (Johnston & Brown, 1984), and in pancreatic β-cells (Atwater *et al.*, 1978; Cook, 1984). The phenomenon of bursting has also been observed in chemical systems such as the Belousov–Zhabotinsky reaction, in conditions close to those that produce aperiodic, i.e. chaotic, oscillations (Hudson *et al.*, 1979).

The origin of bursting behaviour in molluscan neurons has been studied theoretically by Both *et al.* (1976) and by Plant (Plant & Kim, 1976; Plant, 1978), whereas Chay & Keizer (1983, 1985) proposed a model for bursting oscillations of the membrane potential in pancreatic β-cells. Rinzel (1986) further analyzed the latter model and compared it with Plant's model for bursting neurons (Rinzel & Lee, 1986). A three-variable phenomenological model for neuronal bursting was also

0022-5193/87/020219+32 \$03.00/0

proposed by Hindmarsh & Rose (1984). Rinzel & Troy (1982, 1983) addressed the mechanism of bursting in the Belousov-Zhabotinsky reaction by analyzing the model proposed by Janz *et al.* (1980), and explained the phenomenon by means of a piecewise linear map, as also envisaged by Tomita & Tsuda (1980). A recurrent theme in all these theoretical studies is that bursting originates from the coupling of a fast spike-generating mechanism with a slow oscillation (Rinzel & Lee, 1986, Koppel & Ermentrout, 1986).

We have previously observed bursting in a model for a multiply regulated biochemical system (Decroly & Goldbeter, 1982). The model represents the coupling in series of two autocatalytic enzyme reactions. Models of this sort based on a single autocatalytic enzyme reaction have been proposed (Goldbeter & Lefever, 1972; Goldbeter & Segel, 1977) for glycolytic oscillations in yeast and muscle (Frenkel, 1968; Hess *et al.*, 1969) and for the periodic synthesis of cyclic AMP in the slime mould *Dictyostelium discoideum* (Gerisch & Wick, 1975). In addition to bursting, the coupled enzyme system is also capable of presenting aperiodic oscillations and multiple, simultaneously stable, periodic regimes (Decroly & Goldbeter, 1982, 1984*a*,*b*, 1985; Goldbeter & Decroly, 1983). It therefore provides a three-variable prototype for the study of a wide variety of complex patterns of temporal organization in biochemical and other, chemical or biological, systems.

Bursting occurs in the two-enzyme model in a large domain of the parameter space close to a region of chaotic behaviour (Decroly & Goldbeter, 1982). In the domain of bursting, the number of spikes over a period changes in a complex manner with the control parameters. The goal of the present paper is to understand the generation of complex periodic oscillations and the sequence of bifurcations leading from one pattern of bursting to another as well as the transition to chaos. We begin our study by describing, in section 2, the various patterns of simple or complex bursting observed in the three-dimensional system.

Our analysis of the generation of bursts in section 3, is closely related to that of Rinzel (1986). The dynamical evolution of the three variables is separated into two time-scales. We treat the slow variable as a parameter and analyze its influence on the dynamics of the "fast" sub-system. The combination of the fast and slow dynamics gives rise to bursting. In section 4, we analyze a family of one-dimensional return maps obtained by numerical integration of the differential equations which govern the three-variable system. How the shape of the map depends on the system's parameters can be understood qualitatively owing to the separation of the dynamics into two time scales. The analysis of a related, simpler, piecewise linear map in section 5 sheds light on the transition from a bursting pattern with p spikes to a pattern with $p+1$ spikes per period. This transition comprises the passage through highly complex modes of bursting, intertwined in a self-similar manner.

Our analysis permits us to understand the origin of extremely complex modes of periodic behaviour that were first uncovered by direct integration of the system's kinetic equations. For example, the piecewise linear map explains a pattern of complex oscillatory behaviour in which four successive phases of bursting, containing eleven, two, three and two spikes, separated by brief phases of quiescence, are repeated periodically (see also Figs 2(d) and 4(b) in Decroly & Goldbeter, 1982).

We compare our results with the sequences of periodic and aperiodic patterns of bursting obtained by Tomita & Tsuda (1980) for the explanation of experimental data reported by Hudson *et al.* (1979) on complex oscillations in the Belousov–Zhabotinsky reaction. The present study corroborates our previous conclusions (Decroly & Goldbeter, 1985) on the usefulness of one-dimensional return maps for the qualitative understanding of complex modes of oscillatory behaviour in biological systems.

2. Numerical Evidence for Bursting in the Three-variable System

The model enzymatic system (Fig. 1) is governed by the following set of ordinary differential equations

$$\begin{aligned} d\alpha/dt &= v - \sigma_1\Phi(\alpha, \beta) \\ d\beta/dt &= q_1\sigma_1\Phi(\alpha, \beta) - \sigma_2\eta(\beta, \gamma) \\ d\gamma/dt &= q_2\sigma_2\eta(\beta, \gamma) - k_s\gamma \end{aligned} \tag{1}$$

with

$$\Phi(\alpha, \beta) = \alpha(1+\alpha)(1+\beta)^2/[L_1 + (1+\alpha)^2(1+\beta)^2]$$

and

$$\eta(\beta, \gamma) = \beta(1+\gamma)^2/[L_2 + (1+\gamma)^2].$$

Here, parameter v denotes the normalized, constant input of substrate; σ_1 and σ_2 are the normalized maximum activities of enzymes E_1 and E_2, whose allosteric constants are denoted by L_1 and L_2; k_s is the apparent first order rate constant for the removal of product P_2; q_1 and q_2 are constants arising from normalization of the metabolite concentrations (see Decroly & Goldbeter, 1982, for further details).

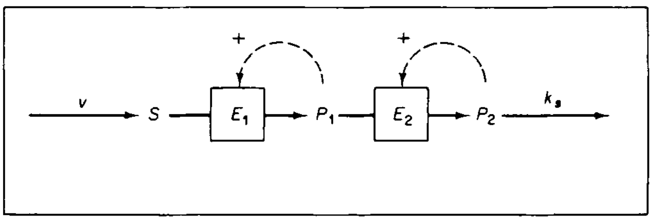

FIG. 1. Model of two autocatalytic enzyme reactions coupled in series, analyzed for bursting behaviour. The time evolution of the three-variable system is governed by eqns (1). The normalized concentrations of S, P_1, P_2 are denoted by α, β and γ in the text.

System (1) will be studied as a function of v and k_s, for the following set of parameter values: $\sigma_1 = \sigma_2 = 10\ s^{-1}$, $q_1 = 50$, $q_2 = 0{\cdot}02$, $L_1 = 5 \times 10^8$, $L_2 = 100$. For these parameter values, the two instability-generating mechanisms associated with the two positive feedback loops present in the model are both active. The first positive feedback loop gives rise to slow oscillations in α and β which are relatively independent of γ, owing to the small value of L_2 (Decroly & Goldbeter, 1982). The second feedback loop produces faster oscillations in β and γ, under the control of the first oscillating mechanism. As shown below, bursting results from the interaction between these two modes of oscillations.

The model has been studied by numerical integration of the differential equations for the variation of two key-parameters, namely, the rate of substrate input, v, and the rate constant for the degradation of the end product, k_s. These parameters govern the input and the output of the system, which, as exemplified by glycolysis (Hess *et al.*, 1969) are readily amenable to experimental control. When bifurcation diagrams are established as a function of k_s, two types of such diagrams can be obtained, depending on the value of v (see Fig. 2 where dark zones indicate chaos,

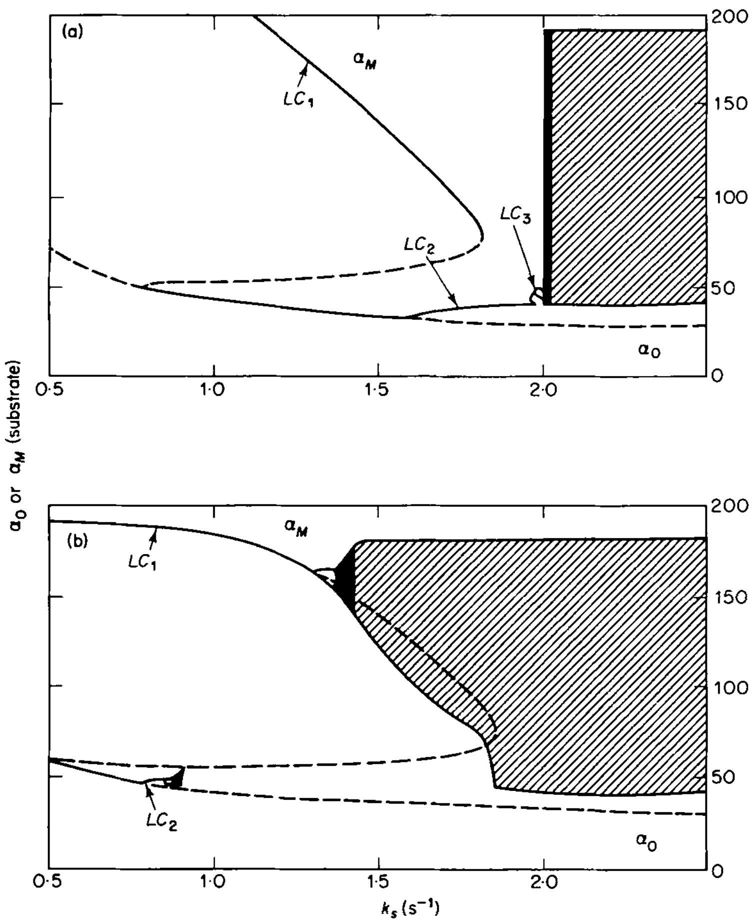

FIG. 2. Bifurcation diagrams obtained for the differential system (1), by the use of program AUTO (Doedel, 1981) supplemented by numerical simulations. We show the behaviour of the system as a function of k_s, for two different values of v: (a) $v = 0{\cdot}45\ s^{-1}$; (b) $v = 0{\cdot}25\ s^{-1}$. Other parameter values are: $\sigma_1 = \sigma_2 = 10\ s^{-1}$, $q_1 = 50$, $q_2 = 0{\cdot}02$, $L_1 = 5 \times 10^8$, $L_2 = 100$. Indicated are the steady-state value, α_0, or the maximum value of α in the course of oscillations, α_M. Stable and unstable solutions are represented by solid or dashed lines, respectively. LC_1, LC_2 and LC_3 refer to stable limit cycles. The dark zone corresponds to chaotic behaviour, whereas the dashed area denotes complex periodic oscillations, i.e. bursting (the envelope of the successive maxima of α is indicated in these zones).

and dashed area denotes complex oscillations in the form of bursting). At large values of v (e.g. $v > 0{\cdot}42\ s^{-1}$), the situation is depicted in Fig. 2(a) (a similar diagram was given in Fig. 1 of Decroly & Goldbeter, 1982). Here, we will focus on the situation that obtains at low values of v (e.g. $v < 0{\cdot}35\ s^{-1}$); this situation is represented in Fig. 2(b), where limit cycle LC_1 loses its periodicity through a sequence of period-doubling bifurcations giving rise to chaotic behaviour following the scenario of Feigenbaum (1978). Upon further increase in k_s, the system undergoes complex oscillations in the form of periodic or aperiodic bursting. The main difference between the two situations considered is that in Fig. 2(b) the transition to chaos and bursting originates on the upper branch of periodic behaviour (i.e. from limit cycle LC_1), whereas it originates on the lower branch (i.e. from limit cycles LC_2 or LC_3) in Fig. 2(a). The transition from the diagram of Fig. 2(a) to that of Fig. 2(b) at intermediate values of v is currently under investigation.

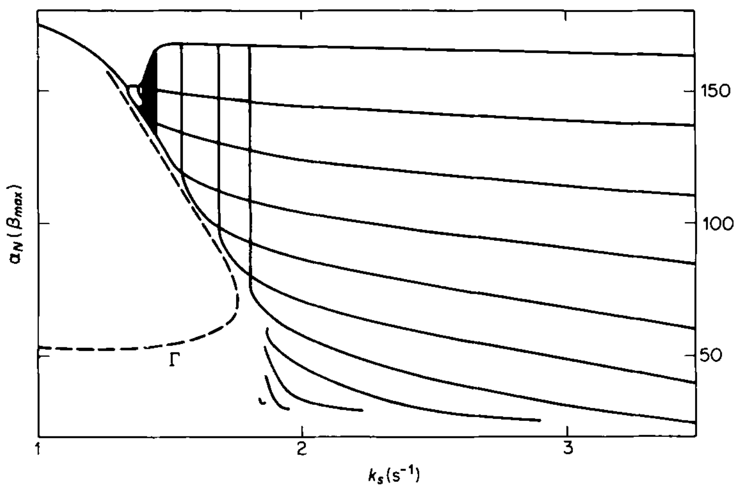

FIG. 3. Bifurcation diagram for the enzymatic system of Fig. 1, showing the variation of the number of spikes per period as a function of parameter k_s, in a region where bursting occurs. For each value of k_s we have plotted the values of α corresponding to successive peaks in β. These values, $\alpha_N(\beta_{max})$ (solid lines) are obtained by numerical integration of eqns (1). Parameter values are those of Fig. 2(b). Dark zones indicate chaotic behaviour or complex bursting patterns of the type $\pi(p, i, j \ldots)$ (see text and Table 1). The dashed line Γ represents the locus of α values for which homoclinic orbits occur in the two-dimensional (β-γ) reduction of system (1), when α is taken as a slowly varying parameter (see section 3).

The situation schematized in the bifurcation diagram of Fig. 2(b) is illustrated in more detail in the region of bursting by the diagram of Fig. 3 obtained by numerical integration of the differential equations. Shown as a function of k_s is the substrate concentration, $\alpha_N(\beta_{max})$, corresponding to a maximum in the value of β during simple or complex periodic oscillations. For a given value of k_s, several values of $\alpha_N(\beta_{max})$ can be observed successively over a period. The number p of these values varies with k_s and corresponds to a bursting pattern comprising p spikes in β over a period. The diagram shows how the bursting pattern changes with k_s. Periodic regimes with $1, 2, \ldots, p, p+1 \ldots$ spikes are found; following Tomita & Tsuda (1980), these will be referred to as $\pi(p)$ modes. At low values of k_s, dark zones indicate domains of chaotic behaviour. Between the modes $\pi(4)$ and $\pi(5)$, $\pi(5)$ and $\pi(6)$, $\pi(6)$ and $\pi(7)$, the dark bands also comprise more complex periodic patterns of bursting of the general form $\pi(p, i, j, \ldots)$, consisting of p spikes followed by i spikes, then j spikes (with $i, j, \ldots$ ranging from 1 to p), the $(p, i, j, \ldots)$ pattern being itself reproduced periodically. An example of the latter behaviour is shown in Fig. 4(e), whereas simpler patterns of bursting are illustrated in Fig. 4(b)-(d). The actual

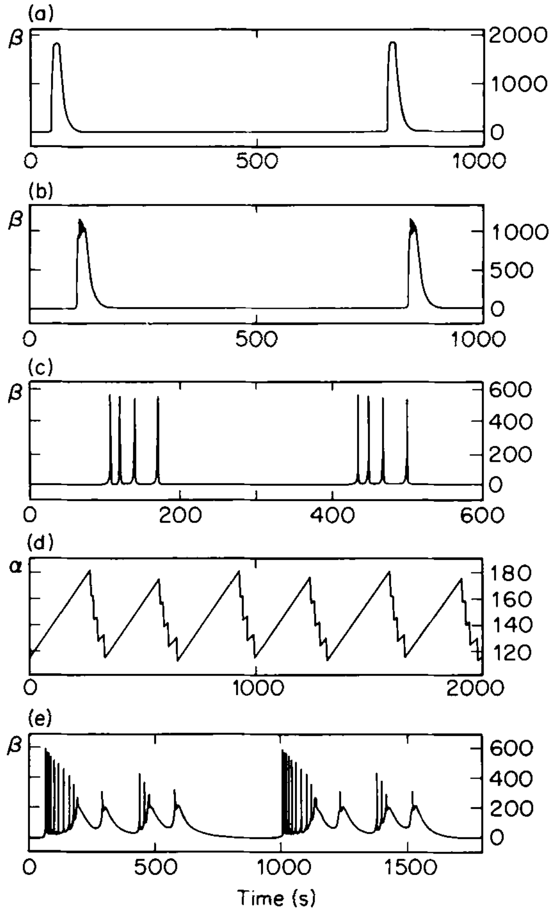

FIG. 4. Patterns of simple or complex oscillatory behaviour in the biochemical system of Fig. 1. Shown are simple periodic oscillations (a) and various patterns of bursting (b-e) represented by the value of β or α as a function of time for different values of v and k_s. (b) and (c) exemplify two markedly different types of simple bursting. In (d), the value of α is shown instead of β so as to better indicate the existence of a periodic $\pi(4, 4)$ mode (see section 5). An example of very complex bursting behaviour is shown in (e). The origin of such complex periodic pattern $\pi(11, 2, 3, 2)$ is explained in sections 5(B) and 5(C) by means of a piecewise linear map. The curves are obtained by numerical integration of eqns (1) for $k_s = 15\ s^{-1}$ (a), $8\ s^{-1}$ (b), $1{\cdot}53\ s^{-1}$ (c), $1{\cdot}534\ s^{-1}$ (d) and $2\ s^{-1}$ (e); $v = 0{\cdot}25\ s^{-1}$ in (a-d) and $v = 0{\cdot}445\ s^{-1}$ in (e). Other parameter values are as in Fig. 2.

TABLE 1

Range of occurrence of the different behavioural modes including chaos and bursting, as a function of k_s, for $v = 0{\cdot}25\ \mathrm{s}^{-1}$; other parameter values are those indicated in Fig. 2(b). Data are obtained by numerical integration of eqns (1). The mode $\pi(i, j)$ represents bursting with a train of i spikes followed by a train of j spikes over a period

$k_s(\mathrm{s}^{-1})$	Behavioural mode	$k_s(\mathrm{s}^{-1})$	Behavioural mode
1·3	$\pi(1)$	1·87	$\pi(11)$
$1{\cdot}34 \le k_s < 1{\cdot}4$	period doubling sequence	1·88	$\pi(10)$
1·4	chaos	1·95	$\pi(10)$
1·4473	$\pi(4)$	1·96	$\pi(9)$
1·532	$\pi(4)$	2·23	$\pi(9)$
1·533	$\pi(4, 4)$	2·24	$\pi(8)$
1·534	$\pi(4, 4)$	2·91	$\pi(8)$
1·535	chaos	2·92	$\pi(7)$
1·5355	$\pi(4, 3)$	4·16	$\pi(7)$
1·536	chaos	4·18	$\pi(6)$
1·537	chaos	5·9	$\pi(6)$
1·5378	$\pi(4, 2)$	6·0	$\pi(5)$
1·544	$\pi(4, 2)$	8·5	$\pi(5)$
1·545	chaos	8·6	$\pi(4)$
1·55	$\pi(4, 1) = \pi(5)$	9·6	$\pi(4)$
1·65	$\pi(5)$	9·7	$\pi(3)$
1·7	$\pi(6)$	10·8	$\pi(3)$
1·8	$\pi(6, 2)$	10·9	$\pi(2)$
1·81	$\pi(7)$	12·5	$\pi(2)$
1·85	$\pi(7)$	12·6	$\pi(1)$
1·86	$\pi(11)$	∞	$\pi(1)$

sequence of $\pi(p)$ modes is given as a function of k_s in Table 1, for the conditions of Fig. 3 (for these parameter values, the most complex patterns of bursting reported are of the type $\pi(p, i)$; the pattern of Fig. 4(e) was found by chance for other values of v and k_s).

The abrupt rise in the number of spikes per period near $k_s = 1{\cdot}8\ \mathrm{s}^{-1}$ is related to the presence of a homoclinic orbit in the two-dimensional $(\beta - \gamma)$ subsystem (the dashed line in Fig. 3 indicates the value of α for which, at a given value of k_s, a homoclinic orbit obtains in the $\beta - \gamma$ subsystem). As shown in Fig. 3, and further explained in section 3 below, this two-dimensional homoclinic orbit plays an essential role in the bursting dynamics of the three-variable system.

The phase space representation of a typical bursting behaviour in the three-variable system is shown in Fig. 5. This figure shows that bursting orginates here from the coupling of a fast spike-generating mechanism with a slow oscillation. Indeed, a limit cycle resulting from the interaction of α and β passes into a region of the phase space where the interactions between β and γ produce rapid oscillations. The resulting trajectory presents the aspect of a "folded" limit cycle (Schulmeister & Sel'kov, 1978). As in previous studies of bursting (see, e.g., Rinzel & Lee, 1986), the existence of distinct time scales permits one to comprehend such complex oscillatory behaviour by analyzing a reduced two-dimensional system.

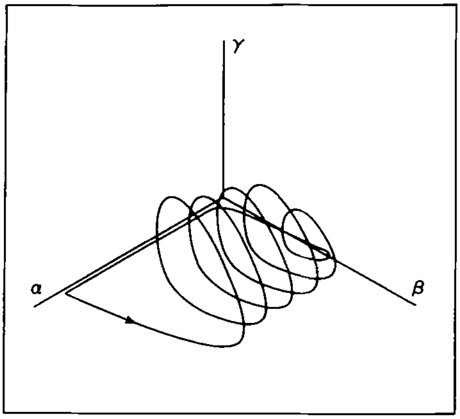

FIG. 5. Phase space representation of *bursting*. Two oscillatory mechanisms are coupled in the three-variable system of Fig. 1, in such a way that the limit cycle induced by the mechanism (α-β) passes in a region of the phase space where the second mechanism (β-γ) produces rapid oscillations. The curve is obtained by integration of eqns (1) for the parameter values of Fig. 2(b) with $k_s = 5\ \mathrm{s}^{-1}$.

3. Bursting: A Two-dimensional Analysis

Numerical simulations show that the dynamics of system (1) during bursting can be separated into two phases. In the first phase, β and γ remain close to the steady state solution of eqns (2a, b)

$$d\beta/dt = q_1\sigma_1\Phi - \sigma_2\eta \tag{2a}$$

$$d\gamma/dt = q_2\sigma_2\eta - k_s\gamma \tag{2b}$$

whereas α slowly increases. In the second phase, β and γ undergo rapid oscillations whereas α slowly decreases. We are thus led to the conclusion that, especially in the second phase, α may be considered as a slow variable when compared to β and γ. This approximation is not as valid during the first phase of bursting, but it is nevertheless supported by the fact that the steady-state solution of eqns (2a, b) is then relatively independent of α. The problem of matching the two phases will not be considered here in further detail.

The slower variation in α allows us to recast the three-variable system (1) in the form of eqns (3) which can be analyzed in the limit $\varepsilon \to 0$.

$$d\alpha/dt = \varepsilon(v' - \sigma_1'\Phi) \tag{3a}$$

$$d\beta/dt = q_1\sigma_1\Phi - \sigma_2\eta \tag{3b}$$

$$d\gamma/dt = q_2\sigma_2\eta - k_s\gamma \tag{3c}$$

where $\varepsilon v' = v$ and $\varepsilon\sigma_1' = \sigma_1$.

The substrate concentration, α, can now be treated as a slowly-varying parameter influencing the dynamics of the fast $\beta - \gamma$ subsystem governed by eqns (3b, c). Strictly speaking, it is clear that the limit $\varepsilon \to 0$ is far from being approached in eqns (3), since v' and σ_1' should then go to infinity. The two-variable approximation nevertheless yields interesting insights into the dynamics of the three-variable system.

By using the program AUTO for the numerical continuation of steady-states and periodic solutions in systems of ordinary differential equations (Doedel, 1981), we have obtained bifurcation diagrams representing the behaviour of the β-γ subsystem as a function of α, for decreasing values of k_s (see Fig. 6). The behaviour of the fast subsystem is indicated by the steady-state value(s) of β, and by the maximum and minimum values of β in the course of oscillations. (Stable and unstable steady or periodic states are represented by solid and dotted lines, respectively.) The actual dynamics of the three variable system is represented by sketching the variation of β as a function of α in the course of time (solid lines with arrows). Notice that, for the sake of clarity, these schematic trajectories are made well distinct from the steady-state branches of β, thus giving the wrong impression that β may take negative values.

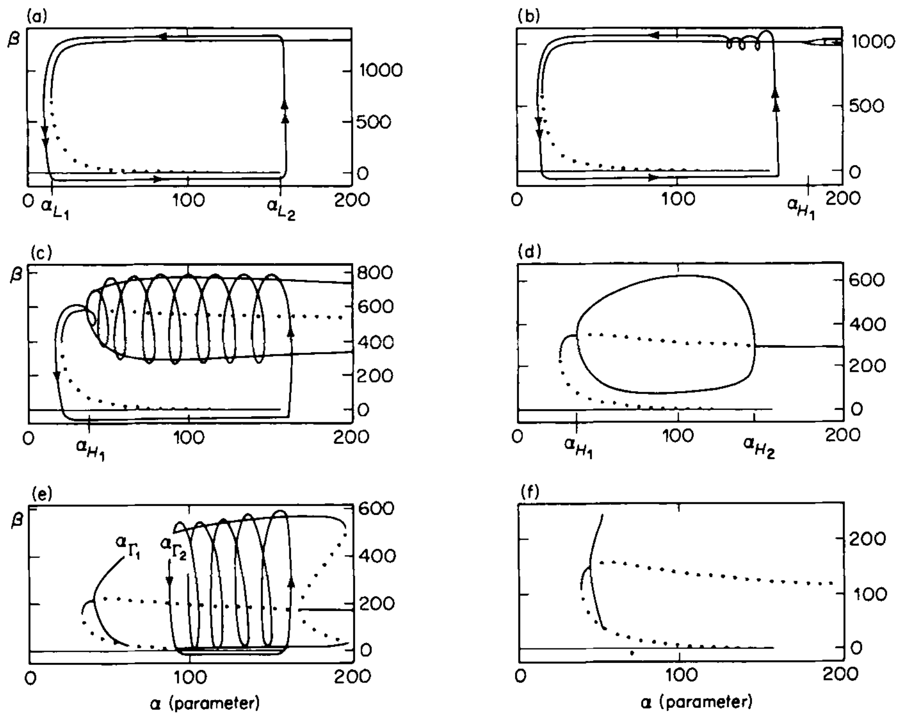

FIG. 6. Bifurcation diagrams of the two-dimensional subsystem β-γ (eqns 2a, b) obtained by use of program AUTO (Doedel, 1981). The steady-state value of β or its maximum value in the course of oscillations are represented as a function of α considered as a parameter, for different values of k_s: $10\,s^{-1}$ (a), $7{\cdot}78\,s^{-1}$ (b), $4{\cdot}5\,s^{-1}$ (c), $2{\cdot}7\,s^{-1}$ (d), $1{\cdot}7\,s^{-1}$ (e), $1{\cdot}2\,s^{-1}$ (f). Solid and dotted lines denote stable or unstable (steady or periodic) regimes. These bifurcation diagrams are independent of v; other parameter values are as in Fig. 2. The behaviour of the three-dimensional system which is schematically represented by the lines with arrows in (a), (b), (c) and (e), can be inferred from these bifurcation diagrams when taking into account the slow variation of α. Also shown are the values of α corresponding to bifurcation points in the two-dimensional (β-γ) system: α_{L_1} and α_{L_2} indicate the limit (turning) points of the hysteresis loop, α_{H_1} and α_{H_2} denote Hopf bifurcations, whereas α_{Γ_1} and α_{Γ_2} are the values for which homoclinic orbits occur.

For low values of α, the steady-state values of β and γ are close to zero. For large values of α, the steady-state value of β is high, and remains practically constant as α increases. Due to the positive feedback exerted by β on enzyme E_1, these two branches of steady-states merge through a hysteresis loop: in a certain range of α values, bounded by two limit points, α_{L_1} and α_{L_2}, the system thus admits three steady-states. For the parameter values considered, the lowest steady-state is always stable (stable node); the intermediate state is always unstable (saddle point), whereas the highest state may be stable or unstable depending on the values of α and k_s. When it is unstable it may be surrounded by a limit cycle, as in Figs 6(c) and 6(d).

The six diagrams of Fig. 6 illustrate different patterns of bursting or simple periodic oscillations. The temporal evolution of the three-variable system can be explained according to these diagrams in the following manner. The rapid variation of β and γ forces the system to stay on the steady-state branch where $d\beta/dt = d\gamma/dt = 0$, except when α reaches one of the limit points of the hysteresis loop. Then, as indicated in Fig. 6, the dynamics is almost vertical since $|d\alpha/dt| \ll |d\gamma/dt| < |d\beta/dt|$. On the lower branch of steady-state, the two enzymes proceed at a low pace as there is almost no reaction, given that β and γ are very low and cannot activate the enzymes; substrate input largely overcomes substrate consumption and α will rise continuously at a rate governed by the constant input of substrate, v. When the system reaches the limit point, α_{L_2}, it jumps abruptly to the upper branch. As β and γ are higher on this branch, both enzymes are activated, in such a way that the reaction transforms α into β and β into γ at a high rate. As a result, the substrate level α decreases and the system moves to the left on the upper branch until it reaches the limit point, α_{L_1}, in which it jumps rapidly to the lower branch. The overall behaviour is thus a simple limit cycle of the relaxation type which is indeed observed for high values of $k_s (> 13\ s^{-1})$ such as in Fig. 6(a), when the steady-state remains a stable node on the two branches of the hysteresis loop in the range $\alpha_{L_1} - \alpha_{L_2}$. For intermediate values of k_s, as in Fig. 6(b), the steady-state on the upper branch becomes unstable through a Hopf bifurcation in $\alpha = \alpha_{H_1} > \alpha_{L_2}$. If α_{H_1} is sufficiently close to α_{L_2}, the steady-state on the upper branch is a stable focus in α_{L_2}. Then, as ε is not strictly 0 in eqns (3), the approach towards the upper branch of steady-states takes the form of a spiral. This results in a *bursting* pattern in which a series of small wiggles, whose amplitude decreases rapidly, occur on the top of a large amplitude oscillation (see Fig. 4(b)).

For lower values of k_s, the Hopf bifurcation point α_{H_1} moves to the left of α_{L_2} and the upper steady-state is an unstable focus surrounded by a stable limit cycle. The domain of oscillation on the upper branch extends from α_{H_1} to a second Hopf bifurcation point, α_{H_2}. In Fig. 6(c), the value of k_s is such that $\alpha_{L_1} < \alpha_{H_1} < \alpha_{L_2} < \alpha_{H_2}$. We then obtain a bursting pattern with a number of large-amplitude spikes in β over a period (Fig. 4(c)). The number of spikes is governed by factors such as the rapidity of evolution on the upper branch (see below) and by the distance between α_{L_1} and α_{H_2}.

In Fig. 6(d), the value of k_s is such that $\alpha_{L_1} < \alpha_{H_1} < \alpha_{H_2} < \alpha_{L_2}$. In such a situation, the amplitude of the spikes in β may in principle pass through a maximum over a period; this is, however, not observed here in a clearcut manner as α_{H_2} remains too close to α_{L_2}.

In $k_s = 1{\cdot}76\ s^{-1}$, the amplitude of the limit cycle on the upper branch has increased to the extent that the limit cycle becomes tangent to the intermediate unstable branch of the hysteresis loop, and thus collides with a saddle point (*homoclinic tangency*). Consequently, two homoclinic orbits appear in the β-γ subsystem for smaller k_s values (Fig. 6(e)). These orbits, which are trajectories that originate from a saddle point and return to it after an infinite time (Guckenheimer & Holmes, 1986), occur for the values α_{Γ_1} and α_{Γ_2}, and move apart as k_s decreases, until only one such orbit remains for $k_s < 1{\cdot}6\ \mathrm{s}^{-1}$ (Fig. 6(f)).

Between α_{Γ_1} and α_{Γ_2}, no stable limit cycle exists on the upper branch and the system evolves to the lower stable branch which remains the only attractor. Then, in the course of bursting, the transition to the lower branch occurs in Fig. 6(e) as α reaches the value α_{Γ_2} rather than α_{L_1} so that the number of spikes diminishes as the accessible oscillatory domain shrinks (birhythmicity has been found in a similar situation in a three-variable model for cAMP oscillations in *Dictyostellium* cells (Martiel & Goldbeter, 1986); the occurrence of such a phenomenon in these conditions has not yet been demonstrated in the present model). The reduction in the number of spikes becomes more and more marked as k_s decreases until bursting disappears altogether. Then a simple limit cycle is established, as shown by the bifurcation diagram of Fig. 3. The latter diagram also indicates that this transition occurs through period doubling bifurcations and chaos.

A further effect of the homoclinic orbit is illustrated in the time evolution shown in Fig. 7. For k_s values slightly above homoclinic tangency ($k_s \approx 1{\cdot}8\ \mathrm{s}^{-1}$), the limit cycle comes very close to the saddle point for intermediate α values (the situation is then intermediate to those depicted in Figs 6(d) and 6(e)). The proximity to the steady-state of the reduced system causes a slowing down of the β-γ oscillations. The pattern of bursting is then characterized by a time interval between successive peaks which passes through a maximum over a period. Such situation of "inverse parabolic" bursting has to be contrasted with the opposite behaviour, referred to

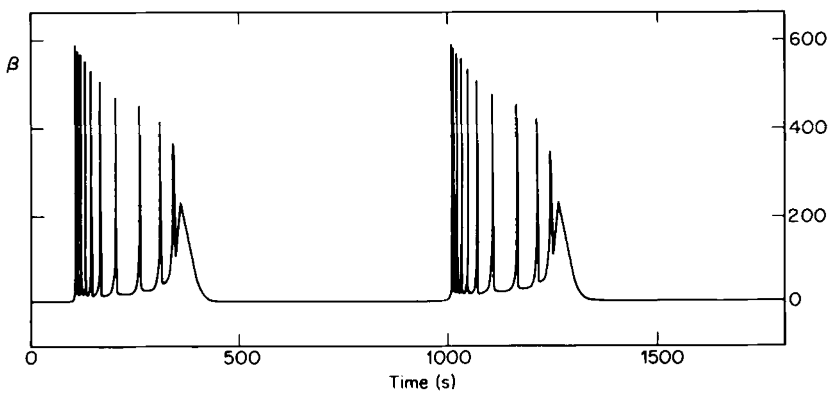

FIG. 7. Temporal behaviour of system (1) obtained for $v = 0{\cdot}25\ \mathrm{s}^{-1}$ and $k_s = 1{\cdot}86\ \mathrm{s}^{-1}$, near the k_s value for which homoclinic tangency occurs in the two-dimensional (β-γ) subsystem. The proximity of the β-γ limit cycle to the unstable saddle point of the two-dimensional subsystem in a situation intermediate between those of Figs 6(d) and 6(e) causes a slowing down of the oscillations in the middle of a train of spikes. As a consequence, the interspike interval passes through a maximum in the course of oscillations, a situation which is referred to in the text as *inverse parabolic bursting*.

as *parabolic bursting*, in which the time interval between successive spikes passes through a minimum over a period (Koppel & Ermentrout, 1986; Rinzel, 1986).

The small-amplitude interburst spikes, which are observed in complex patterns of bursting such as those shown in Fig. 4(e), may also be ascribed to the existence of homoclinic orbits. Such patterns cannot be explained readily by simple considerations of the diagrams in Fig. 6, as it would seem impossible to initiate a train of spikes for values of α below α_{L_2}. Complex patterns of bursting, whose origin will further be discussed in section 5 below, might in fact be due to the slowing down of the β-γ oscillations near homoclinic tangency, possibly when α_{L_1} is close to α_{H_1}. Then indeed, as the evolution becomes "frozen" when β and γ approach the saddle point, substrate input can temporarily exceed substrate consumption, causing one or more series of secondary bursts in β.

The results of the two-dimensional analysis of Fig. 6 are summarized in Fig. 8 which shows as a function of k_s the loci of the limit points α_{L_1} and α_{L_2}, the Hopf bifurcations α_{H_1} and α_{H_2}, and the α values in which homoclinic orbits are observed, α_Γ. The various critical points in the bifurcation diagrams of Fig. 6(a)-(f) can be recovered from Fig. 8 by horizontal sections at the corresponding values of k_s marked a-f. At point D in Fig. 8, the Hopf bifurcation occurs at the value for which the saddle point and the upper state of the hysteresis loop coalesce (i.e. $\alpha_{H_1} = \alpha_{L_1}$). This situation, which corresponds to a double instability in which two conjugate eigenvalues cross the imaginary axis with their imaginary part vanishing simultaneously, gives rise to a homoclinic orbit (Baesens & Nicolis, 1983). Noticeable in this diagram is that the limit point α_{L_2} remains practically unchanged as k_s varies.

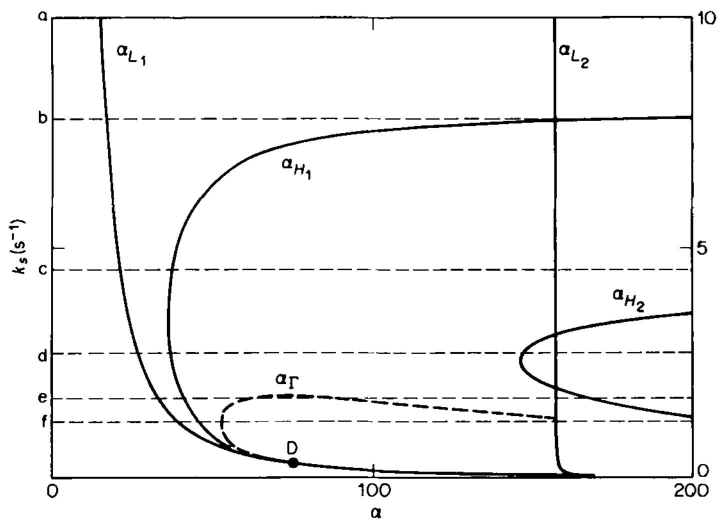

FIG. 8. Behaviour of the two-dimensional β-γ subsystem (2a, b) in the parameter space (α-k_s), obtained by use of program AUTO (Doedel, 1981). This figure summarizes the results presented in Fig. 6. The positions of the lower and upper limit points, the two Hopf bifurcation points, and the presence of the homoclinic orbit are indicated by α_{L_1}, α_{L_2}, α_{H_1}, α_{H_2} and α_Γ, respectively. The dotted lines (a-f) represent horizontal sections through the parameter space for different values of k_s, and correspond to the bifurcation diagrams (a-f) of Fig. 6.

How good a picture of the dynamics of the three-variable system is provided by the two-dimensional reduction depends on the value of parameter ε in eqns (3). A variation in ε corresponds to a simultaneous variation of v, σ_1 and q_1, such that v and σ_1 are changed by the same factor, while the product $q_1\sigma_1$ remains constant. Most of our simulations were initially done for $\varepsilon = 1$, and linear stability analysis shows that the steady-state of the three-dimensional system remains unstable in a limited range above and below this value. For the parameter values considered, with v' ranging from 0·1 to 0·3 s^{-1}, the oscillatory behaviours (including bursting) are only observed for ε values ranging approximately from 0·5 to 2. The contradiction with our taking the limit $\varepsilon \to 0$ is only apparent, as the rate of variation of β and γ are larger than that of α by two and one orders of magnitude, respectively. Appropriate normalization of time in eqns (3) would therefore yield smaller effective values of ε.

The influence of ε is displayed in Fig. 9, where the three-dimensional attractor is shown for $\varepsilon = 0·5$ and $\varepsilon = 2$ (the dynamics for the same parameter values and $\varepsilon = 1$ is shown in Fig. 5). If the motion globally takes place on the same surface, the rate of variation of α (governed by ε), influences the period and the number of spikes in agreement with intuition: the faster α varies, the fewer are the spikes and the shorter is the period. Parameter v by itself does not influence the bifurcation patterns of Fig. 6 as it does not appear in the equations which govern the two-dimensional subsystem (β-γ). Increasing (decreasing) v at constant σ_1 will merely decrease (increase) the period of quiescence separating two successive bursts, by modulating the variation of α.

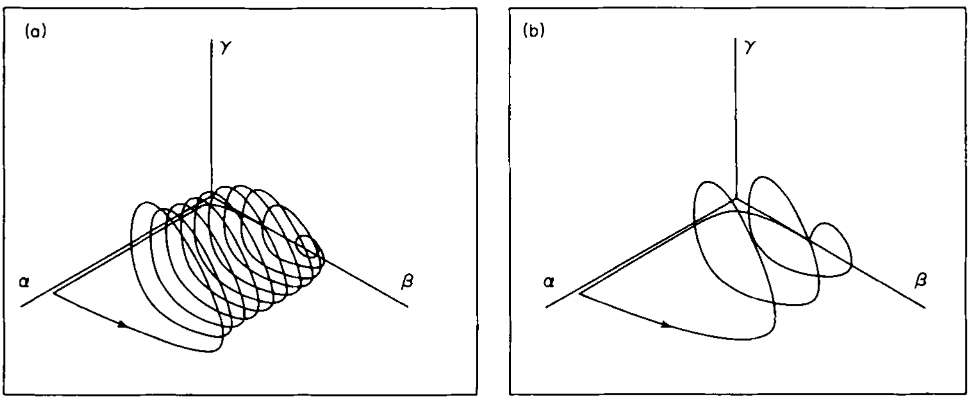

FIG. 9. Phase space representation of the dynamics of system (3) for two different values of ε, 0·5 (a) and 2 (b). Parameter values are: $v' = 0·25\ s^{-1}$, $\sigma_1' = 10\ s^{-1}$, and $k_s = 5\ s^{-1}$; the corresponding parameter values in system (1) are: $v = 0·125\ s^{-1}$, $\sigma_1 = 5\ s^{-1}$ and $q_1 = 100$ (a); $v = 0·5\ s^{-1}$, $\sigma_1 = 20\ s^{-1}$ and $q_1 = 25$ (b). Other parameter values are as in Fig. 5 where $\varepsilon = 1$ in eqns (3).

The above analysis of the two-variable reduction to the fast subsystem (β-γ) controlled by the slowly varying parameter α provides a qualitative explanation for the origin of various patterns of bursting. This analysis does not account, however, for complex oscillatory phenomena such as chaos or period-doubling bifurcations which occur at low values of k_s (see Fig. 3). This is not surprising as the assumption that γ varies more rapidly than α breaks down for such k_s values. The two-variable analysis provides a first approach to the understanding of how the number of spikes or the pattern of bursting depend on the key parameters of the model. Complementary insights can be gained from a further simplification of the dynamics, by consideration of one-dimensional maps.

4. Analysis of a One-dimensional Map Derived from the Three-dimensional System

The reduction of a very dissipative three-dimensional system of ordinary differential equations to a one-dimensional recurrence equation is often used to analyze qualitatively the dynamical behaviour of the original system (Collet & Eckmann, 1980; Gumowsky & Mira, 1980; Shaw, 1980; Kapral *et al.*, 1982; Glass *et al.*, 1983). This method has proved particularly useful for clarifying the structure of the attraction basins in the situation where system (1) possesses two or three periodic attractors (Decroly & Goldbeter, 1985). Such a reduction to a one-dimensional map will be used to understand the complex sequence leading from bursting to chaos. We shall consider first how a map can be obtained by numerical integration of eqns (1). On the basis of these results, we shall construct and analyze, in section 5, a piecewise linear map with closely related characteristics.

The reduction of the dynamical system to a one-dimensional map is only justified in the case of a very dissipative system, since in that case three-dimensional phase-space trajectories rapidly evolve to a nearly two-dimensional sheet on which they remain trapped. The intersections of the trajectories with a Poincaré section transverse to the flow thus show the evolution on a nearly one-dimensional curve. It is then possible to make a one-to-one correspondence between a one-dimensional coordinate on that curve and the place where the three-dimensional trajectory intersects the cross-section. This is generally the case for system (1) (Decroly & Goldbeter, 1985) if the Poincaré section is suitably chosen.

In the course of integrating eqns (1), we construct the map in the following way. Each time β reaches a maximum, we note the value of α: $\alpha_N(\beta_{\max})$. We thus obtain a discrete series of α values, and then plot the $(N+1)$th value as a function of the Nth. Several maps $\alpha_{N+1}=f(\alpha_N)$ are presented in Fig. 10 for different values of the parameters. It is particularly easy to visualize the shape of the map when the dynamical regime is chaotic (Fig. 10(a)), since in such cases the curve is almost continuous. The fact that we obtain a continuous curve for a chaotic dynamics indicates that chaos is deterministic: the behaviour results from a dynamical instability in a deterministic system, and not from statistical noise or numerical errors superimposed on a stable periodic motion.

In situations where bursting occurs, only a few points corresponding to the successive maxima in β are observed since the motion is periodic. A bursting pattern with p peaks per period corresponds to a periodic orbit with p points in the map (see e.g. Fig. 10(b) for a bursting pattern $\pi(4)$ with four spikes per period). Interpolation, realized by joining the points by a smooth curve or by taking several

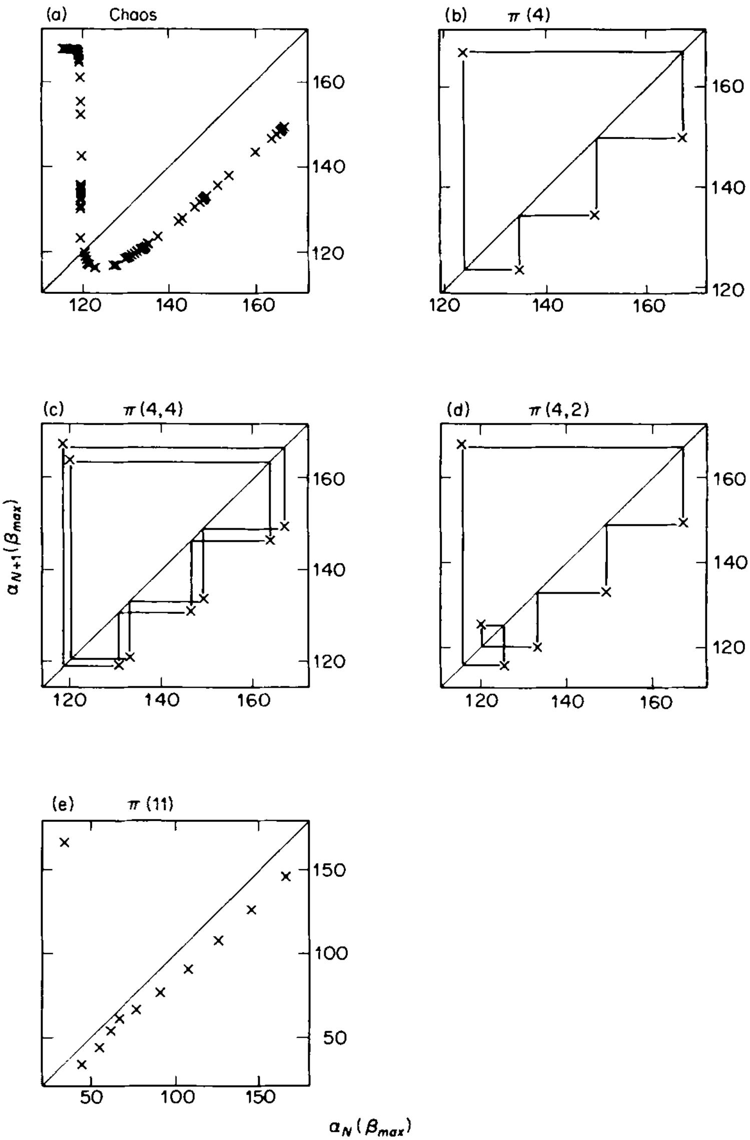

FIG. 10. One-dimensional maps associated with bursting and chaos in the system of Fig. 1. The procedure for the construction of the map $\alpha_{N+1}(\beta_{max}) = f[\alpha_N(\beta_{max})]$ is described in the text (see section 4). Shown are the maps obtained by numerical integration of eqns (1) with the parameter values of Fig. 2(b), for different values of k_s: $1{\cdot}537\ s^{-1}$ (a), $1{\cdot}5\ s^{-1}$ (b), $1{\cdot}534\ s^{-1}$ (c), $1{\cdot}539\ s^{-1}$ (d), $1{\cdot}86\ s^{-1}$ (e). The aperiodic behaviour in (a) gives rise to a continuous curve whereas bursting with p spikes per period corresponds to p points (crosses) on the map. Panels (b) and (e) show maps associated with the simple patterns of bursting $\pi(4)$ and $\pi(11)$; maps corresponding to complex patterns of bursting are shown in (c) and (d). The situations illustrated in (c) and (e) correspond to the time evolution in Figs 4(d) and 7, respectively.

sets of initial conditions far from the asymptotic regime, shows that the shape of the map remains similar to that which is obtained in the chaotic regime. The maps in Figs 10(c) and (d) correspond to more complex patterns of bursting, namely $\pi(4,4)$ (corresponding to the oscillation of Fig. 4(d)), and $\pi(4,2)$, respectively.

The method used here to obtain one-dimensional maps is slightly different from that described in our previous work (Decroly & Goldbeter, 1985). There, the distance from the steady-state to the intersection of the trajectory with a Poincaré cross-section was used as discrete variable. The two methods should be equivalent, at least from a qualitative point of view (Shaw, 1980). We here used $\alpha_N(\beta_{max})$ as discrete variable, because it allows a direct comparison with the results obtained in the preceding sections (see particularly Fig. 6 where the maximum of β is plotted as a function of α).

An important feature of the present model, revealed by the analysis in section 3, is that the jump that initiates a new cycle of bursting after substrate repletion always occurs for α values near the second limit point, α_{L_2}. As shown in Fig. 8, this limit value remains practically independent of k_s. As a result, the first $\alpha_N(\beta_{max})$ value of a new bursting phase generally has the same magnitude, independently of the last $\alpha_{N-1}(\beta_{max})$ value of the preceding train of spikes. This accounts for the horizontal part situated to the left of the well in the map of Fig. 10(a), where $\alpha_{N+1} = \mathbf{M}$ ($\mathbf{M}$ is a constant independent of α_N and relatively insensitive to k_s). This property will be of primary importance for the stability of the orbits as well as for the structure of the transitions from one pattern of bursting to another or from bursting to chaos.

When α has reached its largest maximum, $\mathbf{M}$, which corresponds to the first β-γ cycle after the jump, each oscillation in β-γ will result in removing approximately the same quantity of substrate (denoted $\mathbf{a}$), since the amplitude of oscillations in β remains practically constant in the range of variation of α (see Fig. 6(c)). This is why the right part of the maps is practically linear and parallel to the bisectrix for high α_N values: $\alpha_{N+1} \approx \alpha_N - \mathbf{a}$. For lower α values, the amplitude of the limit cycle decreases as one gets close to the Hopf bifurcation point. Accordingly, the amount of α removed by each cycle is decreased, and the curve gets closer to the bisectrix. The minimum value of α_N corresponds to the return of the system to the lower branch of the hysteresis loop in the diagrams of Fig. 6; the next value, $\alpha_{N+1} = \mathbf{M}$, corresponds to the jump from the lower to the upper branch. Therefore $\mathbf{M}$ is close to α_{L_2}.

Between the left and right parts of the map, numerical simulations in the chaotic regime show a smooth curve joining the two extremes described above. The intersection of the curve with the bisectrix is the fixed point of the map which can be stable or unstable depending on whether the absolute value of the slope of the map is respectively smaller or larger than unity in this point.

Upon parameter variation, the curve transforms smoothly. Understanding how the shape of the map depends on key parameters is particularly useful for the construction of abstract maps carried out in section 5. The influence of parameters v and k_s on the dynamics of the differential system, and hence on the shape of the map, depends on the existence of the homoclinic orbit. When k_s is above the value $1{\cdot}9\ s^{-1}$, i.e. when no homoclinic orbit exists in the two-dimensional subsystem, an increase in k_s produces a decrease in the number of spikes per period (see Fig. 3). In contrast, in the domain of existence of the homoclinic orbit in the two-dimensional system, the number of peaks per period decreases when k_s diminishes.

These opposite effects of k_s on the dynamics can be explained qualitatively by means of one-dimensional maps as follows. Beyond the domain of existence of the homoclinic orbit ($k_s > 1{\cdot}8\ s^{-1}$), an increase in k_s prevents the accumulation of γ. Thus the oscillations in β-γ consume a smaller amount of β as the enzyme E_2 is less activated. The result is a net increase in **a**, the value of α which is removed by each β-γ oscillation as enzyme E_1 is more activated. As shown in section 5, this increase in **a** produces a decrease in the number of peaks over a period. When homoclinic orbits obtain, the decrease in the number of peaks during bursting as k_s diminishes is due to a reduction in the range of α values supporting oscillations in the β-γ subsystem (see Figs 6(e) and 8).

The effect of parameter ε on the dynamics of the system can be comprehended in a similar manner. This parameter governs the rate of variation of α (see eqns (3)). Upon increasing ε, this rate increases and the amount of α consumed over a spike—reflected by the value of **a** in the map—rises. The number of peaks per period therefore decreases when ε increases (see Fig. 9).

No effect of k_s on the maximum value of α, i.e. **M**, can be observed, since, as can be seen in Fig. 8, the position of the lower limit point α_{L_2} is almost unaffected by k_s and, as pointed out previously, $\mathbf{M} \approx \alpha_{L_2}$. Moreover, as the bifurcation diagrams of Fig. 6 are independent of ε, this parameter certainly does not influence the value **M** of the maximum, as long as it remains sufficiently small so that the separation into two time-scales holds for system (3).

That the existence of a homoclinic orbit in the β-γ flow for lower k_s values strongly influences the dynamics of the three-dimensional system has been discussed above and is made clear by Figs 3, 6 and 7. The *bump* in the map of Fig. 10(e) reflects the phenomenon of inverse parabolic bursting shown in Fig. 7. This bump results from the fact that the quantity of α removed by each spike is significantly reduced as the constant input of substrate counterbalances its depletion, since the system spends more time near the saddle where the values of β and γ are low. For lower α values, the removal of α during bursting accelerates together with the motion on the β-γ limit cycle, as the latter moves apart from the saddle. This behaviour also explains the sudden increase in the number of spikes per period, following an increase in k_s near homoclinic tangency (see Fig. 3). Furthermore, in these conditions, for sufficiently large values of v (e.g. $v = 0{\cdot}35\ s^{-1}$), the more rapid substrate input can counterbalance the removal of α due to β-γ oscillations, so that a stable, non-bursting limit cycle is found for k_s values close to the appearance of the homoclinic orbit ($k_s = 1{\cdot}8\ s^{-1}$) (compare also Figs 2(a) and 2(b). This limit cycle is accompanied by only a slight variation in α and mainly originates from the β-γ mechanism of oscillations (see Martiel & Goldbeter (1986) for a similar behaviour in a related biochemical system).

The maps of Fig. 10 provide a simple picture of the oscillatory dynamics of system (1). We have shown that the effect of some key parameters on the shape of these maps can be understood intuitively. This allows us to understand the global features of the generation of bursts and to roughly predict the way in which a variation in key parameters influences the number of spikes per period.

A conspicuous feature of the maps of Fig. 10 is that they are particularly amenable to a piecewise approximation by linear functions. The advantage of piecewise linear maps similar in shape to the maps of Fig. 10, is that they can be readily analyzed, thus leading to qualitative and quantitative predictions that will largely hold for the actual maps and, hence, for the three-dimensional system. In particular, the study of piecewise linear maps will allow us, in the next section, to understand the continuous passage from a pattern of bursting with p spikes to a pattern with $p+1$ spikes per period, following variation of a control parameter. Obtaining complex periodic orbits in the piecewise linear map also throws light on the origin of complex patterns of bursting such as that shown in Fig. 4(e).

5. Analysis of Bursting by means of a Piecewise Linear Map

As explained above, the portions of the map obtained numerically can be approximated at both low and high values of α by linear expressions, corresponding to a horizontal line and to a parallel to the first bisectrix, respectively. For simplicity, we may further approximate the curved central part of the map by a linear function of α joining the other two linear parts. These approximations yield the following piecewise linear map $x_{n+1}=f(x_n)$, represented in Fig. 11

$$x_n \leq 1: \quad x_{n+1}=f_1(x_n)=\mathbf{M} \tag{4a}$$

$$1 < x_n \leq m: \quad x_{n+1}=f_2(x_n)=-\mathbf{b}x_n+\mathbf{b}+\mathbf{M} \tag{4b}$$

$$m < x_n: \quad x_{n+1}=f_3(x_n)=x_n-\mathbf{a} \tag{4c}$$

where the upper bound of the domain of definition of $f_1(x_n)$ is taken, for convenience, as equal to unity, and $\mathbf{m}$ is the abscissa of the minimum of the map, corresponding to the intersection of $f_2(x)$ and $f_3(x)$, i.e.

$$m=(\mathbf{a}+\mathbf{b}+\mathbf{M})/(\mathbf{b}+1) \tag{5}$$

Equations (4) yield the value of x_{n+1} for a given value of x_n. At the next iteration, x_{n+1} is used to generate x_{n+2}. We thus obtain a sequence of values along one dimension which can be seen as the axis of abscissas in Fig. 11; we shall refer to these values as x. Moreover, we shall denote by x_p and pth value of x in a periodic orbit starting in $x_1=\mathbf{M}$.

Notice that the lowest value that can be reached on the map, $\mathbf{m}-\mathbf{a}$, may become negative at large values of $\mathbf{a}$ when $\mathbf{M}$ is small. Such negative values are naturally excluded when X represents a concentration (as in Fig. 10); we shall not worry about this problem, as realistic values of x are readily obtained by a suitable change in coordinates or an appropriate choice of $\mathbf{M}$, $\mathbf{b}$ and $\mathbf{a}$.

Given the simplicity of the piecewise linear approximation, we should not expect a total agreement with the behaviours of the maps obtained numerically. However, as shown in another context by Tomita & Tsuda (1980), due to the similarity in shape between the continuous and piecewise linear maps, the latter nevertheless

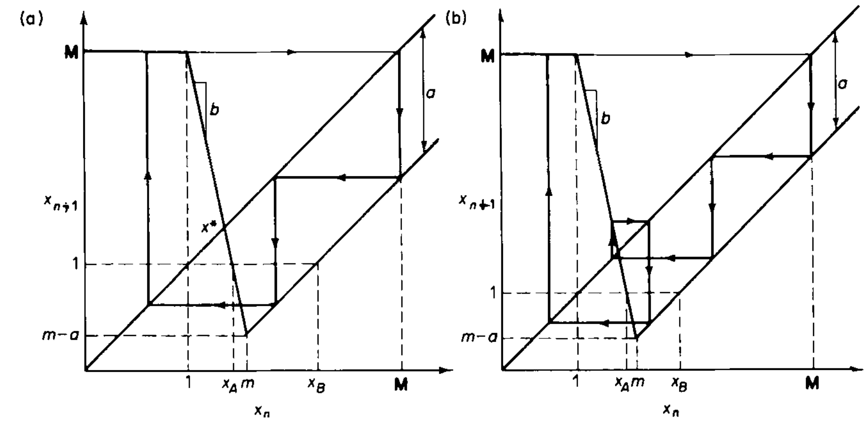

FIG. 11. Piecewise linear map constructed as an approximation of the maps obtained numerically in Fig. 10. The map consists in three segments given by eqns (4a–c) and is controlled by three parameters, **M**, **a** and **b**; m is the abscissa of the minimum of the map, and m-**a** the point to which it iterates. The fixed point x^* is the intersection of the map with the first bisectrix, and is unstable (as it is here) when $\mathbf{b} > 1$. Points falling between x_A and x_B are constrained to iterate in two steps to $x = \mathbf{M}$, as the left part of the map, corresponding to f_1 in eqn (4) is horizontal. The thin solid line with arrows shows the trajectory corresponding to a bursting pattern $\pi(3)$ in (a) and $\pi(3, 2)$ in (b). Parameter values are $\mathbf{b} = 5$, $\mathbf{M} = 11$, with $\mathbf{a} = 6$ in (a) and $\mathbf{a} = 4{\cdot}3$ in (b).

provide a qualitative explanation for the sequence of bifurcations leading from $\pi(p)$ to $\pi(p+1)$ bursting patterns. The detailed analysis developed below shows that this sequence contains more complex patterns of bursting, of the type shown in Fig. 4(e). To our knowledge, such patterns have not previously been described.

(A) CONSTRAINED PERIODIC ORBITS (CPOs): ORIGIN OF STABLE $\pi(p)$ MODES

When $\mathbf{M} > 1$, the fixed point x^* of the map, where $x_{n+1} = x_n$, ($x^* = f(x^*)$), is located on its central segment (eqn 4b). The fixed point $x^* = (\mathbf{b}+\mathbf{M})/(\mathbf{b}+1)$, is unstable provided that the absolute value of the slope, $|-\mathbf{b}|$, is larger than one. In such a case, let us follow the dynamics of the map when starting in $x_1 = \mathbf{M}$ (thin solid line with arrows in Fig. 11). At each iteration, the abscissa of the representative point will decrease stepwise from **M** by the quantity **a** (eqn 4c), thus giving a sequence $x_p = \mathbf{M} - (p-1)\mathbf{a}$. This goes on as long as the abscissa of x_{p-1} remains larger than m. When x_{p-1} becomes smaller than m, the next point x_p is given by either eqn (4a) or eqn (4b) depending on whether x_{p-1} is smaller or larger than unity.

An essential feature of the map is that the set of the points x_p located below unity shrinks to a single point as all these points iterate to a single value, $x_{p+1} = \mathbf{M}$, which is the initial point. We thus obtain a periodic orbit of period p, given by the general eqn (6)

$$f(x_1) = x_2, f(x_2) = x_3, \ldots f(x_p) = x_1 \equiv \mathbf{M}. \tag{6}$$

The points of this periodic orbit correspond to fixed points of the pth iterate of the map, i.e.

$$f^p(x_1) = x_1, f^p(x_2) = x_2, \ldots f^p(x_p) = x_p. \tag{7}$$

Whether the fixed points given by eqn (7) are stable depends on the absolute value of the derivative of $f^p(x)$ in these points. By using the chain rule and eqn (6), we obtain

$$(f^p(x_1))' = \ldots = (f^p(x_p))' = f'(x_1) \,.\, f'(x_2), \ldots f'(x_p) \tag{8}$$

Thus, a periodic orbit given by eqn (6) is stable as long as condition (9) holds

$$\left| \prod_{i=1}^{i=p} f'(x_i) \right| < 1. \tag{9}$$

A trajectory starting from $x_1 = \mathbf{M}$ which arrives at $x_p < 1$ and therefore goes back to $x_{p+1} = \mathbf{M}$ is always stable since $f'(x_p) = f'(\mathbf{M}) = 0$. We refer to such trajectories as *constrained periodic orbits* (CPOs). The CPOs represent superstable orbits (Collet & Eckmann, 1980) as they pass through a point where the slope of the map is nil. However, the present map contains a finite domain—rather than a single point—where the slope is nil. As a consequence, we obtain here CPOs over a large range of parameter values whereas superstable orbits occur only for particular parameter values in maps admitting a curved extremum (Kapral *et al.*, 1982).

CPOs exist only if the ordinate, (m-$\mathbf{a}$), of the minimum of the map is below unity, which condition, by means of eqn (5), takes the form

$$\mathbf{a} > (\mathbf{M} - 1)/\mathbf{b}. \tag{10}$$

If the constraint (10) applies, the domain of points that iterate towards values of x lower than one is bounded by the two preimages of $x = 1$ (i.e. the points iterating in one step to $x = 1$) (see Fig. 11). The abscissas, x_A and x_B, of these points are given by eqn (11)

$$x_A = (\mathbf{M} + \mathbf{b} - 1)/\mathbf{b}, \qquad x_B = \mathbf{a} + 1. \tag{11}$$

For given values of $\mathbf{a}$, $\mathbf{b}$ and $\mathbf{M}$, the map admits at most one CPO. Depending on the parameter values, one observes simple or complex CPOs on the map,

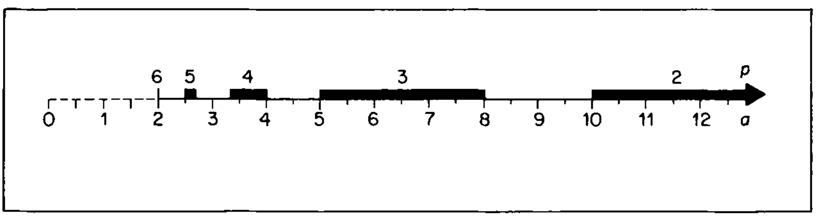

FIG. 12. Domains of $\mathbf{a}$ values for which periodic $\pi(p)$ modes—i.e. simple CPOs—exist in the map given by eqn (4). For the fixed values $\mathbf{b} = 5$, $\mathbf{M} = 11$, we find these orbits as explained in section 5(A) by taking into account eqn (11) and solving the inequality $x_A \leq x_{p-1} \leq x_B$, where x_{p-1} is given by eqn (12a) (see also Fig. 11). The dotted line below $\mathbf{a} = 2$ corresponds to a region where the constraint (10) does not apply. Then, the minimum of the map is above 1 and the jump to $\mathbf{M}$ will never occur, so that simple or complex CPOs are excluded; only unstable periodic orbits or chaos obtain in these conditions. The thick lines are the loci of existence of the simple periodic modes $\pi(p)$ (the values of p are indicated above these lines). The periodic mode $\pi(2)$ extends until $\mathbf{a} = \infty$, as the maximum $\mathbf{M}$ iterates directly to a value comprised between x_A and x_B. Complex CPOs obtain in the intervals between $\pi(p)$ modes (see Figs 13 and 14).

Page 238: In line 10 of the caption to Fig. 12 replace "a value comprised between x_A and x_B." with "a value lower than one."

corresponding to simple or complex bursting patterns. Simple CPOs, denoted $\pi(p)$, obtain whenever the $(p-1)$th descending iterate of $x_1 = \mathbf{M}$ falls between x_A and x_B. More complex CPOs denoted $\pi(p, i, j, \ldots)$, occur when the representative point moves down p times along the right part of the map (4c), and is reinjected upwards on the central part of the map (4b), without passing between x_A and x_B (see Fig. 11b). Then, it decreases i times on the right part of the map ($i \le p$, since the starting point is then lower than $\mathbf{M}$), falls again outside the constraint, is reinjected upwards, decreases for j iterates ($j \le p$) ... until it finally falls between x_A and x_B. It then iterates to $\mathbf{M}$ and thereby completes the CPO. Depending on the parameter values, the period of such orbits can be arbitrarily long, as the trajectory may undergo a large number of cycles before landing in $\mathbf{M}$. There exist isolated values of the parameters such that no CPO obtains; trajectories then lead either to an unstable cycle, or end up in the unstable fixed point x^*. Whether or not truly aperiodic orbits may occur in the piecewise linear map for particular parameter values has not been demonstrated.

Upon increasing $\mathbf{a}$, as the distance between x_A and x_B increases most trajectories will sooner or later enter the interval bounded by x_A and x_B, thus giving rise to a stable, simple or complex CPO. We can construct explicitly all the successive points of simple CPOs of period p, corresponding to bursting patterns with p spikes. These orbits are of two kinds which differ by the last term, x_p before the jump to $x_{p+1} \equiv x_1 = \mathbf{M}$.

When $m \le x_{p-1} \le x_B$, starting from $x_1 = \mathbf{M}$, the successive points of the CPO $\pi(p)$ are given by

$$\begin{aligned}
x_1 &= \mathbf{M} \\
x_2 &= x_1 - \mathbf{a} = \mathbf{M} - \mathbf{a} \\
&\cdots \\
x_{p-1} &= x_{p-2} - \mathbf{a} = \mathbf{M} - (p-2)\mathbf{a} \\
x_p &= x_{p-1} - \mathbf{a} = \mathbf{M} - (p-1)\mathbf{a}.
\end{aligned} \tag{12a}$$

On the other hand, when $x_A \le x_{p-1} \le m$, the successive points $x_1, \ldots, x_{p-1}$ are still given by eqn (12a), but the last point now obeys eqn (12b)

$$\begin{aligned}
x_p &= -\mathbf{b}x_{\mathbf{p}-1} + \mathbf{M} + \mathbf{b}. \\
&= -\mathbf{b}(\mathbf{M} - (\mathbf{p}-2)\mathbf{a}) + \mathbf{M} + \mathbf{b}.
\end{aligned} \tag{12b}$$

In periodic orbits of the type (12a), all points $x_1, \ldots, x_p$ decrease successively by an equal amount $\mathbf{a}$. This is also true for the $(p-1)$ first points in orbits of the second type (12b), but the last point then decreases by a smaller amount comprised between $\mathbf{a}$ and $(\mathbf{M}-1)/\mathbf{b}$.

We can now determine the domain of existence of the successive $\pi(p)$ periodic modes as a function of $\mathbf{a}$ (Fig. 12). For fixed values of $\mathbf{M}$ and $\mathbf{b}$, combining eqns (11) and (12), one obtains the values of $\mathbf{a}$ such that x_{p-1} is comprised between x_A and x_B. These values of $\mathbf{a}$ correspond to the domain of existence of a CPO with p points per period. In the case considered in Fig. 12, the values of $\mathbf{M}$ and $\mathbf{b}$ are such that the maximum value $p=6$ is reached in $\mathbf{a}=2$, for which $x_A=x_B$. Then, the CPO obtains for a single value of $\mathbf{a}$. This CPO can be reached only from an initial point belonging to the cycle, or from an initial value below unity which iterates to $\mathbf{M}$.

Values of p larger than 6 can be obtained for other values of $\mathbf{M}$ and $\mathbf{b}$. Furthermore, the minimum value of p is always *two* since at large values of $\mathbf{a}$, the trajectory starts in $\mathbf{M}$, falls once on the branch $x_{n+1}=x_n-\mathbf{a}$, before returning to $\mathbf{M}$. As the distance between x_A and x_B increases with $\mathbf{a}$, the successive domains of $\pi(p)$ modes in Fig. 12 grow larger with this parameter. Simple periodic patterns $\pi(1)$, i.e. non-bursting limit cycles, correspond to a stable fixed point of the map and therefore appear in the piecewise linear map only when $\mathbf{b}<1$.

The decrease in the number of points per period following an increase in $\mathbf{a}$ corresponds to the decrease in the number of spikes per period observed in the three-dimensional system for values of k_s above homoclinic tangency when k_s or ε are raised, given that $\mathbf{a}$ increases with both parameters (see sections 3 and 4).

(B) ORIGIN OF COMPLEX PATTERNS OF BURSTING $\pi(p, i)$ BETWEEN $\pi(p)$ AND $\pi(p+1)$ MODES

A conspicuous feature of the diagram of Fig. 12 is that the domains of existence of periodic $\pi(p)$ modes are not contiguous. Tomita & Tsuda (1980) found a similar situation in their interpretation of the experiments on complex oscillations and chaos in the Belousov-Zhabotinsky reaction. These authors showed on a piecewise linear map that the periodic bursting modes $\pi(p)$ and $\pi(p+1)$ are separated by modes characterized by a periodic or random alternance between p and $p+1$ spikes. The situation encountered here is different. How a continuous increase of the parameter $\mathbf{a}$ leads from a periodic regime $\pi(p+1)$ to $\pi(p)$ is the next step of our investigation.

Upon increasing $\mathbf{a}$ the following patterns are successively observed by numerical iteration of the map (4)

$$\pi(p+1), \chi, \pi(p,2), \chi, \pi(p,3), \ldots, \chi, \pi(p,p-1), \chi, \pi(p,p), \pi(p). \qquad (13)$$

In the sequence (13), $\pi(p, i)$ represents a periodic pattern formed by p decreasing values of x starting from $\mathbf{M}$, followed by i distinct, decreasing values, starting from a new maximum value of x smaller than $\mathbf{M}$, whereas χ stands for more complex orbits of longer period (see section 5(c) below).

The $\pi(p)$ periodic mode disappears upon a *decrease* in $\mathbf{a}$ because the abscissa of the last point of the orbit, x_p moves from the left to the right of x_B. Then, the next point x_{p+1} is slightly lower than $\mathbf{M}$. As a consequence, x_{p+p} will be lower than x_B. Thus, as the $\pi(p)$ periodic pattern disappears, a new periodic mode $\pi(p,p)$ appears: $\pi(p)$ doubles its period upon a decrease in $\mathbf{a}$. The two successive sequences of p points differ by the location of these points on the map. An example of such behaviour in the differential system (1) is shown in Fig. 4(d) for a $\pi(4, 4)$ bursting pattern; the associated map in Fig. 10(c) indicates that the slight differences in the location of the points on the map correspond to slight differences in the amplitude of α during oscillations. This phenomenon yields time-series reminiscent of the period-doubling phenomenon described by Feigenbaum (1978). However, the two phenomena should be distinguished, since no further period-doubling occurs in the piecewise linear map upon a further decrease in **a**. It will be shown below in the analysis of more complex CPOs that the passage from $\pi(p)$ to $\pi(p, p)$ corresponds to the addition of p points to a simpler orbit rather than to a period-doubling bifurcation.

Further understanding of the origin of the complex transition (13) can be gained from the diagram presented in Fig. 13. There, for the fixed values $\mathbf{b}=5$ and $\mathbf{M}=11$ considered in Fig. 12, we have plotted as a function of **a**, the significant features of the piecewise linear map

(i) $x=x_A$ and $x=x_B$, the abscissas which limit the domain (shaded area) in which the points iterate in two steps towards **M**; also indicated is $x=1$, i.e. the point to which x_A and x_B both iterate;

(ii) $x=m$, the abscissa of the minimum of the map, and its iterate, $x=m-\mathbf{a}$ (dashed lines); $m-\mathbf{a}$ is the lowest value of x that can be reached in the course of time.

According to eqns (12), we then plot as a function of **a**, the straight lines (dotted or solid) $x_1=\mathbf{M}$, $x_2=\mathbf{M}-\mathbf{a}, \ldots, x_p=\mathbf{M}-(p-1)\mathbf{a} \ldots$ which correspond to the p first points of a trajectory starting in **M**. To comprehend the dynamics of the system, we may draw a vertical line corresponding to a given value of **a**. The points where this line intersects the lines $x_1, \ldots, x_p$, are the successive values of x decreasing on the right part of the map, when starting from $x_1=\mathbf{M}$. Of importance is the fact that

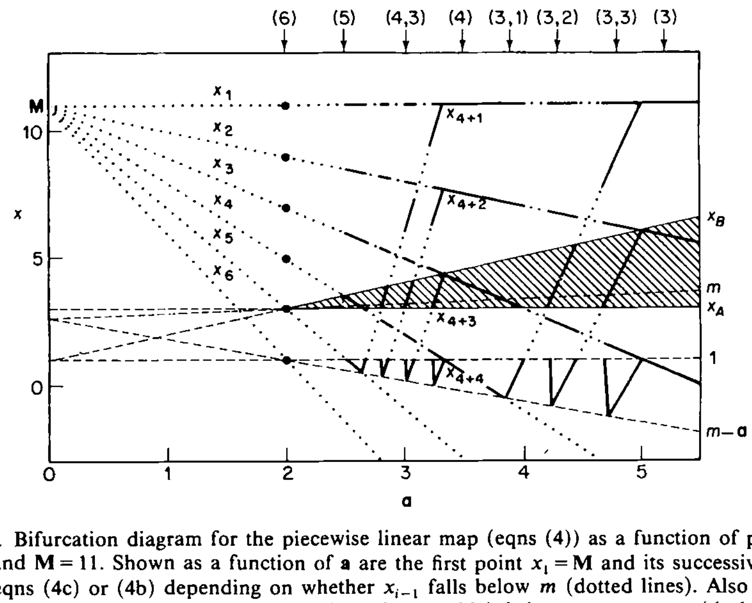

FIG. 13. Bifurcation diagram for the piecewise linear map (eqns (4)) as a function of parameter **a**, for $\mathbf{b}=5$ and $\mathbf{M}=11$. Shown as a function of **a** are the first point $x_1=\mathbf{M}$ and its successive iterates x_i given by eqns (4c) or (4b) depending on whether x_{i-1} falls below m (dotted lines). Also shown as a function of **a** are the minimum, $x=m$, and the point to which it iterates, $x=m-\mathbf{a}$ (dashed lines). A simple or complex CPO occurs as soon as a point in a trajectory originating from **M** enters the dashed area between the lines $x=x_A$ and $x=x_B$ which corresponds to the domain of points iterating in two steps towards **M** (see text for details). The segments corresponding to the successive points of a CPO are represented by heavy lines. As in Fig. 12, the CPO $\pi(6)$ (heavy dots) occurs in $a=2$. The diagram illustrates the transition from $\pi(5)$ to $\pi(4)$ and from $\pi(4)$ to $\pi(3)$. The procedure explained in the text, shows that between $\pi(5)$ and $\pi(4)$ there exist the more complex periodic patterns $\pi(4, 1)$, $\pi(4, 2)$, $\pi(4, 3)$ and $\pi(4, 4)$. Some of the simple and complex CPOs are indicated on top of the figure, for particular values of **a**.

each point whose abscissa is comprised between x_A and x_B will have an ordinate—corresponding to the next iterate—comprised between $(m-\mathbf{a})$ and 1. These next points having abscissas lower than one will automatically iterate towards $x=\mathbf{M}$ and will thereby complete a periodic orbit of the CPO type. The locus of existence of the $\pi(p+1)$ CPO appears therefore in Fig. 13 as the range of $\mathbf{a}$ values for which the straight line $x_p=\mathbf{M}-(p-1)\mathbf{a}$ passes through the dashed area situated between x_A and x_B. Over this range of $\mathbf{a}$ values, all x_p lines are drawn as solid lines to indicate the existence of a CPO (each of the $x_1,\ldots,x_p$ points indeed belongs to the periodic orbit). A few examples of such CPOs of the type $\pi(p)$ or $\pi(p,i)$ have been indicated on the top of Fig. 13, for particular values of $\mathbf{a}$.

The two different types of periodic orbit, corresponding to (12a) and (12b) are encountered successively when increasing $\mathbf{a}$: the CPO (12a) lasts as long as the line corresponding to x_p, i.e., $x_p=\mathbf{M}-(p-1)\mathbf{a}$ is situated above $x=m$. The next point is given by $x_{p+1}=x_p-\mathbf{a}$. Upon increasing $\mathbf{a}$, this point moves downwards on the next line corresponding to x_{p+1}, until it reaches the minimum of the map, $m-\mathbf{a}$, as x_p arrives in m.

When x_p is located below m and above unity (as soon as $x_p=1$, the new periodic mode $\pi(p)$ appears), the next iterate takes place on the central part of the map. Upon a further increase in $\mathbf{a}$, this point, given by eqn (12b) as $x_{p+1}=-\mathbf{b}[\mathbf{M}-(p-1)\mathbf{a}]+\mathbf{M}+\mathbf{b}$, moves upwards along a line of slope $\mathbf{b}(p-1)$. This line of x_{p+1} values starts in $x_{p+1}=m-\mathbf{a}$ for the value of $\mathbf{a}$ for which $x_p=m$, and arrives in $x_{p+1}=\mathbf{M}$ for the value of $\mathbf{a}$ for which $x_p=1$. In Fig. 13, an example of such line (marked x_{4+1}) is shown for the transition from $\pi(5)$ to $\pi(4)$. For $\mathbf{a}$ values such that x_{p+1} is situated on that line, below $x=1$ (x_p is then comprised between x_A and m), the simple CPO $\pi(p+1)$ continues to obtain, obeying eqn (12b). As the line escapes the domain bounded by x_A and x_B (shaded area), when $x_{p+1}>1$, the $\pi(p+1)$ mode disappears and complex modes of behaviour (denoted χ in (13)) are observed.

As $\mathbf{a}$ further increases, the point x_{p+1} (exemplified by the line x_{4+1} in Fig. 13) continues to move upwards along the same line and is now located above one. Finally, x_{p+1} falls itself between x_A and x_B and a new periodic mode, $\pi(p,2)$, appears as x_{p+2} (exemplified by the line x_{4+2}) moves below unity. This periodic mode also involves two distinct types of orbits depending on whether the last point of the orbit is given by eqn (4b) ($x_A<x_{p+1}<m$) or (4c) ($m<x_{p+1}<x_B$). This mode disappears when $\mathbf{a}$ increases, because x_{p+1} becomes larger than x_B, so that $x_{p+2}=x_{p+1}-\mathbf{a}$ moves above unity.

Upon further increase in $\mathbf{a}$, x_{p+2} moves upwards, and falls in turn in the dashed area bounded by x_A and x_B. Then, a new CPO appears, denoted $\pi(p,3)$. The mechanism is repeated until the CPO $\pi(p,p)$ appears. The latter mode finally disappears as the $\pi(p)$ mode is restored, as described above, upon an increase in $\mathbf{a}$. In sequence (13), for reasons of continuity, the pattern $\pi(p+1)$ might in fact be viewed as a pattern $\pi(p,1)$. As indicated in Fig. 13 for the patterns $\pi(4)$ and $\pi(3,1)$, we may consider that a complex CPO $\pi(p,\ldots,i)$ transforms formally into $\pi(p,\ldots,i-1,1)$ as soon as the last point of the orbit before the jump to $\mathbf{M}$ moves from the right part to the central part of the map (the same distinction applies to simple CPOs obeying eqns (12a) or (12b)). The difference between $\pi(p,i-1,1)$

and $\pi(p, i)$ may be tenuous, as the transition occurs in a continuous manner. Thus in Fig. 12, we did not make the distinction between $\pi(p, 1)$ and $\pi(p+1)$—e.g. between $\pi(3, 1)$ and $\pi(4)$. Similarly, in the differential system it may be difficult to distinguish a complex pattern with a group of 6 spikes followed by a single spike from a pattern with 7 spikes.

The "bifurcation diagram" of Fig. 13 can be further understood by translating the process of iteration in the map for a fixed value of **a**, to the iteration of segments of straight lines representing in Fig. 13 the loci of successive iterates of the map as a function of **a**. As pointed out above, a CPO obtains whenever one such segment falls in the dashed area comprised between x_A and x_B.

A segment of straight line of slope $-(p-1)$ thus represents as a function of **a**, the locus of the points x_p of orbits starting in $x_1 = \mathbf{M}$. The part of this segment which is situated above $x = m$ evolves towards a next segment of line, locus of x_{p+1}, of slope $-(p)$, whereas the part of the segment of x_p values situated between $x = m$ and $x = 1$ iterates to a segment x_{p+1} of slope $-\mathbf{b}[-(p-1)]$, joining $x = m - \mathbf{a}$ to $x = \mathbf{M}$ in the same range of **a** values. The same iteration process can be applied to the latter segment in order to generate the loci of the subsequent iterates of the map. The part of the locus of x_{p+1} situated above m, evolves to x_{p+2} values according to eqn (4c), yielding a segment of slope $-\mathbf{b}[-(p-1)]-1$. On the other hand, the part of the segment of x_{p+1} values situated below m, which iterates according to eqn (4b), evolves towards a segment of slope $-\mathbf{b}\{-\mathbf{b}[-(p-1)]\}$, to which we can apply the same reasoning to find the segments of $x_{p+3}, x_{p+4}, \ldots, x_{p+n}$ values. In Fig. 13, we have only plotted the first iteration in the process which displays explicitly the succession of complex CPOs in sequence (13), for the transition from $\pi(5)$ to $\pi(4)$ and from $\pi(4)$ to $\pi(3)$.

The part of a segment of solution of a given slope **s**, situated below m, is mapped by eqn (4b) to a segment of steeper (since $|\mathbf{b}| > 1$) but inverted slope, $-\mathbf{bs}$. This process yields the locus of the next point in a complex CPO. Each time this process applies, an additional excursion to higher ($<\mathbf{M}$) x values occurs; when the corresponding segment is comprised between x_A and x_B, such reinjection gives rise to a complex periodic orbit characterized by an additional index $(i, j, \ldots)$ in the CPO. As the slope of these segments of iterates given by eqn (4b) rises geometrically as $(-\mathbf{b})^n$ with the number n of reinjections, the domain of **a** values for which these segments fall between x_A and x_B—and hence the domain of existence of very complex CPOs—shrinks exponentially. The parameter **b** thus governs the rate of shrinking of the domains of existence of very complex CPOs. As **b** increases, the very complex patterns become more difficult to observe.

(C) HIGHLY COMPLEX PATTERNS OF BURSTING $\pi(p, i, j \ldots)$ AND SELF-SIMILARITY

The sequence (13) for the transitions encountered between $\pi(p)$ and $\pi(p+1)$ can be analyzed in further detail. Between $\pi(p, i)$ and $\pi(p, i+1)$, the reasoning outlined above shows that, upon an increase in **a**, there obtains a sequence (14)

$$\pi(p, i), \chi, \pi(p, i, p), \chi, \pi(p, i, p-1), \chi, \ldots, \pi(p, i, 2), \chi, \pi(p, i+1). \quad (14)$$

Sequence (14) resembles sequence (13) as the same process of mapping of a segment has been utilized to find the next iterate, as well as the domains of existence of complex CPOs. However, the order in which the successive periodic modes are encountered is inverted due to the multiplication of the slope of the segment x_{p+1} by $-\mathbf{b}$. The transition to the mode $\pi(p, i, p)$, resulting from the addition of p points to the mode $\pi(p, i)$ is equivalent, at this level of complexity, to the transition from $\pi(p)$ to $\pi(p, p)$ in (13). The phenomenon should henceforth be distinguished from a period-doubling bifurcation, since at the level of (14) such a bifurcation should yield a transition from $\pi(p, i)$ to $\pi(p, i, p, i)$.

The transitions between $\pi(p)$ and $\pi(p, p)$, and between $\pi(p, i)$ and $\pi(p, i, p)$ differ from each other in another respect. The geometrical properties of the map are such that, as explained above, the $\pi(p)$ mode transforms directly into $\pi(p, p)$ as $\mathbf{a}$ is decreased. On the contrary, at higher degrees of complexity of the CPOs, due to the additional excursions on the central part of the map, the properties allowing for the direct transition between $\pi(p)$ and $\pi(p, p)$ no longer hold. Consequently, very complex orbits denoted by χ are found between $\pi(p, \ldots, i)$ and $\pi(p, \ldots, i, p)$ as indicated in sequences (14) and (15).

We show in Fig. 14(a) the sequence of CPOs denoted a–g, obtained by numerical iteration of the map (4) (with $\mathbf{b}=7$ and $\mathbf{M}=11$), for the passage from $\pi(6, 2)$ (a) to $\pi(6, 3)$ (g). The CPOs obtained at this level of resolution for $\mathbf{a}$ obey sequence (14). Figure 14(b) represents an enlargement of a detail of Fig. 14(a) revealing the structure of the complex orbits χ comprised between the CPOs $\pi(6, 2, 5)$ (c) and $\pi(6, 2, 4)$ (d). This shows that a cloud of points (χ) in Fig. 14(a) resolves into a set of CPOs with an additional index; these orbits, denoted i–m, are themselves separated by bands of even more complex CPOs (χ) which will be resolved in a similar manner upon further magnification. The comparison of the two figures demonstrates the self-similarity properties of the sequence of CPOs: the level of complexity is higher in Fig. 14(b), but the transition between periodic orbits in the two figures is governed by the same rule. The general sequence of CPOs is given by either (15a) or (15b) depending on whether the number of indices in the CPO $\pi(p, i, \ldots, j, n)$ is odd or even, respectively

$$\pi(p, i, \ldots, j), \chi, \pi(p, i, \ldots, j, p), \chi, \pi(p, i, \ldots, j, p-1), \chi, \ldots,$$
$$\pi(p, i, \ldots, j, 2), \chi, \pi(p, i, \ldots, j+1) \tag{15a}$$

$$\pi(p, i, \ldots, j+1), \chi, \pi(p, i, \ldots, j, 2), \chi, \ldots, \pi(p, i, \ldots, j, p-1), \chi,$$
$$\pi(p, i, \ldots, j, p), \chi, \pi(p, i, \ldots, j). \tag{15b}$$

Notice that sequences (13) and (14) are obtained from the generalized sequences (15b) or (15a), respectively, when setting the number of indices equal to two or three.

In principle the rescaling process illustrated in Figs 14(a), (b) can be applied indefinitely so that infinitely complex CPOs may occur in the map, corresponding to π patterns with an infinite number of indices. However, as shown in Figs 14(a), (b), and as pointed out in section 5(B) the domain of occurrence of a complex CPO decreases markedly as the degree of complexity rises. If n denotes the number of indices in the pattern $\pi(p, i, j, \ldots)$ the size of the domain of $\mathbf{a}$ values corresponding

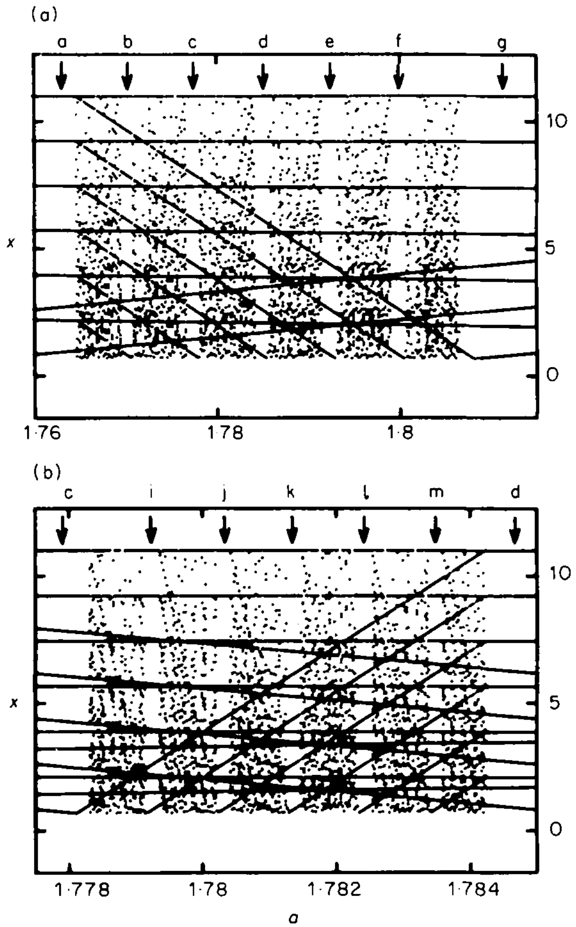

FIG. 14. Self-similarity in the sequences of complex bursting patterns in the piecewise linear map. The bifurcation diagrams are obtained numerically when iterating eqn (4) with **b** = 7, **M** = 11, as a function of **a**, for the passage from $\pi(6, 2)$ to $\pi(6, 3)$ (a) and from $\pi(6, 2, 5)$ to $\pi(6, 2, 4)$ (b). (b) represents an enlargement of a small portion of panel (a). The comparison of the two panels indicates self-similarity in structure. At each level of complexity (i.e. for each additional index in the pattern $\pi(p, i, j, \ldots)$) the direction of change of the last index is reverted (see eqns (15a) and (15b)). To construct these diagrams, the dynamic behaviour of the map is determined for 300 increasing values of **a**. Starting from the initial value $x = \mathbf{M}$, transients are allowed to die out, as the map is iterated 50 times before the values of x for 30 successive steps are plotted. Periodic modes $\pi(6, 2)$, $\pi(6, 2, 6)$, $\pi(6, 2, 5)$, $\pi(6, 2, 4)$, $\pi(6, 2, 3)$, $\pi(6, 2, 2)$ and $\pi(6, 3)$ are indicated by a to g in (a) for particular values of **a**. Between these modes, more complex periodic orbits are obtained for smaller parameter domains as shown in (b) where the transition from $\pi(6, 2, 5)$ to $\pi(6, 2, 4)$—i.e. from c to d in (a)—is shown to contain the modes $\pi(6, 2, 4, 2)$, $\pi(6, 2, 4, 3)$, $\pi(6, 2, 4, 4)$, $\pi(6, 2, 4, 5)$ and $\pi(6, 2, 4, 6)$ indicated by i to m for particular values of **a**. Enlargement of a band of complex CPOs in (b) would yield a similar picture with even more complex periodic orbits. Notice that lines appearing in (a) and (b) result here from numerical iterations rather than from analytical expressions as in Fig. 13.

to such pattern varies as $\mathbf{b}^{-n}$, and therefore rapidly becomes vanishingly small if $\mathbf{b}$ is large, i.e. if the central part of the map is steep. As the central part of the maps obtained numerically is very steep (see Fig. 10), we do not expect to find, over wide domains of parameter values, very complex CPOs in the differential system (1). Such solutions do however occur, as illustrated in Fig. 4(e).

The sequences (15) are only obtained for the piecewise linear map when the left part corresponding to f_1 in eqn (4) is strictly horizontal. When f_1 is not horizontal, complex periodic orbits which pass several times on the part of the map corresponding to f_2, where the absolute value of the slope is bigger than one, become unstable (see eqn (9)) when the slope of f_1 is different from zero, provided that they contain a sufficient number of points on the central part of the map. The most complex CPOs are destroyed in such conditions and replaced by aperiodic (*chaotic*) orbits.

Other non-constrained periodic orbits which do not pass by $\mathbf{M}$ can be found when the initial point x_1 in eqn (12) differs from $\mathbf{M}$ and lies on the central part of the map, f_2. These orbits are always unstable in the piecewise linear map. They could be stabilized in the case of a curved nonlinear map similar to the maps obtained numerically for system (1) (see Fig. 10), if one point of the orbit falls sufficiently near the minimum of the map, where the slope is zero. In such a case, if a CPO exists for the same parameter values, one could observe two stable periodic orbits in the map. This birhythmicity would correspond to the coexistence between two different bursting patterns, in a narrow range of parameter values. Such birhythmic behaviour would differ from that previously described (Decroly & Goldbeter, 1982), in which two simple, simultaneously stable limit cycles coexist; the latter situation would be associated with the coexistence of two stable fixed points in the map (Decroly & Goldbeter, 1985).

(D) A MORE REALISTIC ABSTRACT MAP

When we compare the results obtained for the piecewise linear map with those obtained for a map given by a continuous nonlinear curve, some novel features appear. The sequence of period-doubling bifurcations observed for low k_s values in Fig. 3 cannot be accounted for by the piecewise linear map, since in the latter case no period-doubling occurs.

In Fig. 15, we present a bifurcation diagram obtained for an abstract nonlinear map, which matches more closely the shape of the maps numerically obtained in Fig. 10, but still resembles the piecewise linear map given by eqn (4). This map, represented by the inset in Fig. 15 obeys eqns (16)

$$x_n \le x_j: \quad x_{n+1} = g_1(x_n) = \mathbf{M} \tag{16a}$$

$$x_n > x_j: \quad x_{n+1} = g_2(x_n) = [x_n^2 - (\mathbf{A}+1)x_n + \mathbf{B}]/(x_n - 1), \tag{16b}$$

where x_j is the value of x such that $g_2(x_j) = \mathbf{M}$.

The map is constructed so as to possess a vertical asymptote in $x = 1$ and an asymptote of slope 1, $x_{n+1} = x_n - \mathbf{A}$. In such a manner, the main characteristics of the maps numerically obtained by integration of eqns (1) are preserved as in the piecewise linear map ($\mathbf{A}$ plays here the role of $\mathbf{a}$ in the map (4)), but the central

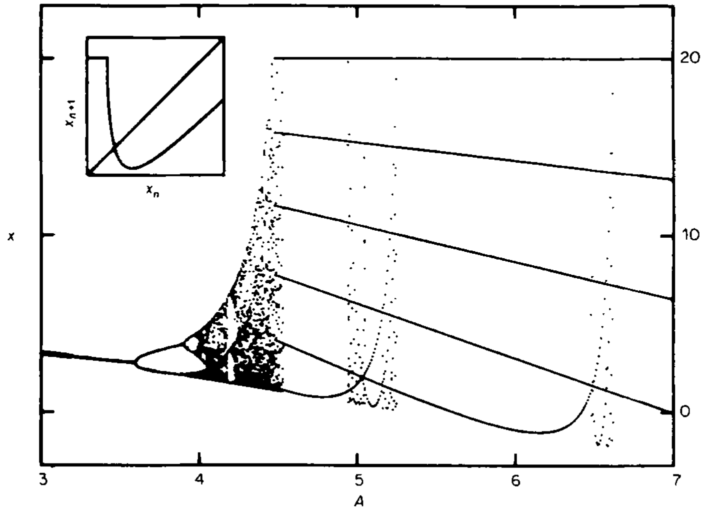

FIG. 15. Bifurcation diagram for the nonlinear map. The diagram is obtained as in Fig. 14, by iterating eqns (16) with **M** = 20 and **B** = 7 for different values of **A**. This map (see inset) qualitatively matches the maps of Fig. 10. The bifurcation diagram resembles that established in Fig. 3 for the original system of differential equations (1).

well becomes curved rather than angular. The value of x_j, solution of a second degree equation is slightly larger than 1 so that the map is continuous, given the existence of an asymptote in $x = 1$.

As shown in Fig. 15, which is obtained by iterating numerically the map (16), upon increasing **A** successive period-doubling bifurcations leading to chaos occur before CPOs are obtained. This can be easily understood, since the minimum of the map given by eqn (16b) is locally quadratic. Upon changing the parameter values, the dynamical behaviour on the map (16) should undergo a sequence of period-doubling bifurcations according to the analysis of Feigenbaum (1978), as soon as the slope of the map becomes smaller than -1 at the fixed point. The sequence of period-doubling bifurcations in the nonlinear map (Fig. 15) matches the similar sequence obtained in the three-dimensional system (1) (Figs 2 and 3). As in the piecewise linear map (4), it is the horizontal, left part of the map (16) which is responsible for the occurrence of simple and complex CPOs at larger values of **A**. This constraint, by imposing an upper bound on the value of x, yields periodic trajectories which would otherwise be chaotic. The sequence of CPOs in the nonlinear map still obeys the transition rules (15) and, as in the piecewise linear map, bands of complex CPOs possess a self-similar structure.

Figure 15 accounts qualitatively for the bifurcation diagram of Fig. 3 in the range of k_s values situated above homoclinic tangency; it provides an intuitive link between the latter numerical diagram and Fig. 13 which was obtained by means of an abstract piecewise linear map.

The fact that the map (16) is nonlinear prevents a detailed analytical treatment, and therefore justifies the use of the piecewise linear map. The detailed analysis of the latter map allows us to understand qualitatively the sequence of complex periodic oscillations corresponding to complex bursting patterns in system (1). In particular, the analytical bifurcation diagrams of Figs 13 and 14 explain how bursting phenomena of the type $\pi(p, i, j, \ldots)$ can be obtained. An example of such complex CPO in the differential system (1) is shown in Fig. 4(e). The piecewise linear approach further explains the transition between different complex patterns of bursting, as a function of parameter values. However, the chaotic behaviour as well as the sequence of period doubling bifurcations cannot be explained by the piecewise linear map given by eqns (4). Such phenomena may be accounted for by nonlinear maps such as that obeying eqn (16).

6. Discussion

We have presented a qualitative explanation for the generation of complex periodic oscillations (bursting) in a multiply regulated biochemical system. Such oscillations were first observed by numerical simulations of a set of three ordinary differential equations not amenable to detailed analytical treatment. Our analysis of bursting rests on successive, complementary approaches which correspond to progressive simplification of the original model. It is noteworthy, and somewhat paradoxical, that these simplifications in fact allow one to see complex modes of oscillatory behaviour not easily perceived in the original system of differential equations.

The first approach, analogous to that developed by Rinzel (1986) and Rinzel & Lee (1986) for the analysis of membrane potential bursting, consists in the separation of the three-dimensional dynamics into fast and slow time-scales. The analysis then reduces to that of a two-variable system, in which the third variable becomes a slowly varying parameter. Such analysis yields bifurcation diagrams for the fast β-γ subsystem as a function of the third variable α taken as a parameter whose slow variation gives rise to bursting. Some of the bifurcation diagrams obtained here present a striking resemblance to those obtained by Rinzel (1986) for bursting of membrane potential in nerve cells and in pancreatic β-cells, and by Martiel & Goldbeter (1986) for bursting and birhythmicity in a model for cAMP oscillations in *Dictyostelium* cells.

The two-variable analysis shows how complex oscillations develop from simple periodic behaviour upon variation of a control parameter (see Fig. 4). It also accounts for the occurrence of different types of bursting, namely, small-amplitude wiggles at the top of slower, large-amplitude oscillations (Fig. 4(b)), or groups of large-amplitude spikes separated periodically by quiescent phases (Fig. 4(c)). Both types of bursting are known to occur in chemical and biological systems. Moreover, the separation between fast and slow subsystems sheds light on the origin of "inverse parabolic" bursting in which the time interval between successive spikes passes through a maximum. This behaviour occurs just before the onset of a homoclinic orbit in the fast subsystem.

The next step in the reduction consists in obtaining a one-dimensional return map that reflects the behaviour of the differential system. The analysis of a related piecewise linear map then allows us to understand the complex sequence of bifurcations leading from a periodic pattern with p spikes to one with $p+1$ spikes per period. This transition from $\pi(p)$ to $\pi(p+1)$ involves the passage through domains of more complex periodic regimes: $\pi(p, p)$, $\pi(p, p-1), \ldots, \pi(p, 2)$, $\pi(p, 1)$, interspersed with even more complex periodic oscillations in a self-similar manner (see Figs 14(a), (b)). Another instance of self-similarity was previously described in the present model, for the fractal structure of the attraction basins in the case of the coexistence between two stable limit cycles separated by unstable chaos (Decroly & Goldbeter, 1984*b*, 1985).

The occurrence and stability of *constrained periodic orbits* (CPOs) in the piecewise linear map arise from the fact that the left segment of the map is horizontal. Upon slight deviation from horizontality the more complex CPOs disappear and give way to chaos. Another form of chaos preceded by period-doubling bifurcations is obtained in a nonlinear map which more closely resembles the map associated with the time evolution of the differential system. The sequence of complex CPOs is given by the same rules as in the piecewise linear map, and also possesses properties of self-similarity. The behaviour of the nonlinear map thus accounts for both the sequence of complex bursting patterns and for the chaotic dynamics observed in the model.

The complex patterns of oscillations of the type $\pi(p, i, j, \ldots)$ obtained in the piecewise linear map account for—and explain the origin of—similar bursting oscillations observed in the differential system (see e.g., Fig. 4(e)). Such patterns did not appear in the sequence analyzed by Rinzel (1986), who described periodic bursting with $1, 2, \ldots n, n+1, \ldots$ spikes, but did not investigate in detail the transition between these bursting patterns.

On the other hand, Tomita & Tsuda (1980) have used the reduction to a one-dimensional map to understand the sequence of bursting oscillations observed experimentally in the Belousov-Zhabotinsky reaction by Hudson *et al.* (1979). They depicted a transition which shares some similarities with the sequence described here, as it also implies a transition between periodic modes $\pi(p)$ and $\pi(p+1)$. There, however, the transition is characterized by modes of behaviour corresponding to a periodic or chaotic alternance between p and $p+1$ spikes.

The predictions obtained by the one-dimensional analysis remain qualitative as there is no precise relation between the parameters of the model and those of the maps. Nonetheless, the analysis of one-dimensional maps has already explained the structure of the attraction basins when system (1) admits more than one stable periodic attractor (Decroly & Goldbeter, 1985). Such analysis, supplemented by that of a piecewise linear map, have allowed us here to understand the sequence of complex periodic oscillations observed by numerical integration of the enzymatic model, as well as to explain the existence of very complex patterns of bursting oscillations in some ranges of parameter values.

Bursting neurons, pancreatic β-cells, *Dictyostelium* amoebae, and the present biochemical system share, in spite of their diversity, common properties of temporal organization. Although the time evolution of these systems is governed by markedly different kinetic equations, the bifurcation diagrams obtained by separating their dynamics into two time scales indicate a common origin for bursting behaviour. In a similar manner, the sequence of bursting patterns obtained here upon variation of a control parameter may hold for a variety of dynamical systems, as the shape of the maps investigated here may well arise in other bursting systems. Of particular significance is the fact that Chay and Rinzel (1985) have obtained a one-dimensional map similar to the one obtained here, but inverted in shape, in their study of bursting in a model for the pancreatic β-cell. The present analysis may thus be of general relevance to bursting phenomena in chemistry and biology, even if the differential equations considered specifically relate to enzyme kinetics.

We wish to thank P. Gaspard, J. L. Martiel, G. Nicolis, J. Rinzel and X. J. Wang for fruitful discussions, and E. J. Doedel for communicating to us the program AUTO. One of the authors (O.D.) is Aspirant du Fonds National Belge de la Recherche Scientifique (F.N.R.S.).

REFERENCES

ALVING, B. O. (1968). *J. gen. Physiol.* **51**, 29.
ADAMS, W. A. & BENSON, J. A. (1985). *Progr. Biophys. Mol. Biol.* **46**, 1.
ATWATER, J., RIBALET, B. & ROJAS, E. (1978). *J. Physiol., Lond.* **278**, 117.
BAESENS, C. & NICOLIS, G. (1983). *Z. Phys.* **52B**, 345.
BOTH, R., FINGER, W. & CHAPLAIN, R. A. (1976). *Biol. Cybernetics* **23**, 1.
CHAY, T. R. & KEIZER, J. (1983). *Biophys. J.* **42**, 181.
CHAY, T. R. & KEIZER, J. (1985). *Biophys. J.* **48**, 815.
CHAY, T. R. & RINZEL, J. (1985). *Biophys. J.* **47**, 357.
COLLET, P. & ECKMANN, J.-P. (1980). *Iterated Maps on the Interval as Dynamical Systems.* Basel and Boston: Birkhäuser Verlag.
COOK, D. L. (1984). *Fed. Proc.* **43**, 2368.
DECROLY, O. & GOLDBETER, A. (1982). *Proc. natn. Acad. Sci. U.S.A.* **79**, 6917.
DECROLY, O. & GOLDBETER, A. (1984*a*). *C.R. Acad. Sci. Paris Ser. II* **298**, 779.
DECROLY, O. & GOLDBETER, A. (1984*b*). *Phys. Lett.* **105A**, 259.
DECROLY, O. & GOLDBETER, A. (1985). *J. theor. Biol.* **113**, 649.
DOEDEL, E. J. (1981). (Proc. 10th Manitoba Conf. on Num. Math. and Comput., Winnipeg, Canada) *Cong. Num.* **30**, 265.
FEIGENBAUM, M. J. (1978). *J. Stat. Phys.* **19**, 25.
FRENKEL, R. (1968). *Arch. Biochem. Biophys.* **125**, 151.
GERISCH, G. & WICK, U. (1975). *Biochem. Biophys. Res. Commun.* **65**, 364.
GLASS, L., GUEVARA, M. R., SHRIER, A. & PEREZ, R. (1983). *Physica* **7D**, 89.
GOLDBETER, A. & DECROLY, O. (1983). *Am. J. Physiol.* **245**, R478.
GOLDBETER, A. & LEFEVER, R. (1972). *Biophys. J.* **12**, 1302.
GOLDBETER, A. & SEGEL, L. A. (1977). *Proc. natn. Acad. Sci. U.S.A.* **74**, 1543.
GUCKENHEIMER, J. & HOLMES, P. (1986). *Nonlinear Oscillations, Dynamical Systems and Bifurcations of Vector Fields*, 2nd edn. Berlin: Springer.
GUMOWSKI, I. & MIRA, C. (1980). *Dynamique Chaotique.* Toulouse, France: Ed. CEPADUES.
HESS, B., BOITEUX, A. & KRÜGER, J. (1969). *Adv. Enzyme Regul.* **7**, 149.
HINDMARSH, J. L. & ROSE, R. M. (1984). *Proc. R. Soc. Lond. B*, **221**, 87.
HUDSON, J. L., HART, M. & MARINKO, D. (1979). *J. chem. Phys.* **71**, 1601.
JANZ, R. D., VANACEK, D. J. & FIELD, R. J. (1980). *J. chem. Phys.* **73**, 3132.
JOHNSTON, D. & BROWN, T. H. (1984). In: *Electrophysiology of Epilepsy*, p. 277. London: Academic Press.
KAPRAL, R., SCHELL, M. & FRASER, S. (1982). *J. Phys. Chem.* **86**, 2205.
KOPPEL, N. & ERMENTROUT, G. B. (1986). *Math. Biosci.* (in press.)
MARTIEL, J. L. & GOLDBETER, A. (1986). *Lect. Notes in Biomath.* (in press.)
PLANT, R. E. (1978). *Biophys. J.* **21**, 217.
PLANT, R. E. & KIM, M. (1976). *Biophys. J.* **16**, 227.
RINZEL, J., (1986). In: *Proc. 6th Dundee Conf. on the Theory of Ordinary and Partial Differential Equations.* (Sleemann, B. D., Jarvis, R. J. & Jones, D. S. eds) Basel and Boston: Springer.
RINZEL, J. & LEE, Y. S. (1986). In: *Nonlinear Oscillations in Biology and Chemistry*, (Othmer, H. G. ed.) p. 19. Berlin: Springer Verlag.
RINZEL, J. & TROY, W. C. (1982). *J. chem. Phys.* **76**, 1775.
RINZEL, J. & TROY, W. C. (1983). *Contemp. Math.* **17**, 411.
SCHULMEISTER, T. & SEL'KOV, E. E. (1978). *Stud. Biophys.* **72**, 111.
SHAW, R. (1980). *Z. Naturforsch.* **36a**, 80.
TOMITA, K. & TSUDA, L. (1980). *Prog. theor. Phys.* **64**, 1138.